PRELIMINARY INVESTIGATIONS OF PHYSICAL
MEASUREMENT CORRELATIONS WITH CURING
TREATMENTS OF PEANUTS

1960 - 1961

by
Richard C. Fluck

June 1961
Raleigh, North Carolina

TABLE OF CONTENTS

Introduction

Peanuts subjected to high temperatures during the curing process develop objectionable flavor characteristics. This "off-flavor" has not been exactly correlated with any physical measurements. Taste tests give only subjective evaluations and the causative substance has not yet been isolated and analyzed chemically. It is suspected that physical qualities such as hardness and brittleness are caused by improper curing treatment. Excessive splitting of peanut kernels has been correlated with rapid drying. Obviously both physical and chemical changes occur in the drying kernel. It is hoped that curing treatment can be correlated with physical measurements for the purpose of easy detection and for further knowledge of structure and composition of the peanut kernel.

For these reasons a program has been initiated between Best Foods, Division of Corn Products Co., and the Agricultural Engineering Department of North Carolina State College. The primary objective of this program is to "correlate various physical measurements with observable quality characteristics and known curing treatments". This is the objective toward which the writer has been working. The program has thus far fallen into three phases of work. These are a literature survey, preliminary investigations into three areas, and hardness investigations.

Literature Survey

The first phase of work encompassed a literary survey of all known work in the field relating to curing practices causing undesirable effects on the peanut kernel or derivative products. This gave the writer a cognizance of work that had been done, gaps existing in the knowledge of the subject, and ideas concerning approaches to the problem. The study delved into physical properties which might be both measurable and significant of any structural or compositional changes in the peanut during curing. Electrical and magnetic properties, optical properties, thermal properties, sonic qualities, density, viscosity, hardness, elastic properties, and brittleness were considered as being possible measurements upon peanut kernels or derivative products. These expand into innumerable individual measurements. Obviously many had to be rejected on the basis of a suspected lack of measurable differences or on the basis of previous work. (It was felt that the writer might duplicate experience already gained in light transmittance characteristics, for instance.)

Preliminary Investigations

Preliminary investigations into a few physical character-
istics occupied the second phase of the investigation. Peanuts
cured in air at room temperature and at 120° F were used to
represent two extremes of curing treatments in these tests.
Determination of dielectric constant and of fluorescent response
using available equipment gave no measurable differences or
encouragement, and these areas were not pursued further. Di-
electric constant determinations were made upon a paste of finely
ground peanuts. Fluorescent response curves were obtained from
the paste and from peanut butter. Dielectric constant measure-
ments were made at one kilocycle frequency. Fluorescent response
was determined using a modified Beckman DU Spectrophotometer at
wavelengths between 400 mu and 550 mu. All response curves were
similiar.

Measurements of the density of the kernels from these two
treatments, however, gave encouraging results. E. O. Beasley and
J. W. Dickens had made observations of the differences of flotation
characteristics in water. This approach had also been taken by
T. A. Pickett and K. T. Holley at the University of Georgia using
dry sand as a volume filler material. Their results showed a
definite correlation between specific volume and curing temperature
of the whole peanut due to the changing void space between the
cotyledons. The writer used a Jolly spring balance for measuring
weights and water as the volume filler. The measurements were made
quickly and it was assumed that no water was absorbed by the kernels.

First results show not only that there is indeed a difference
between the "apparent density" of the whole kernel but also
a possible difference in the actual density of the separate
cotyledons due to differences in temperature. Further investi-
gations are planned in this area to determine the densities of
peanuts and of separate cotyledons cured over a range of curing
treatments. It is planned also to determine whether or not
any water is absorbed by the peanuts during the test. A simple
objective test based on specific volume differences can probably
be evolved. It might possibly be a flotation test using a series
of solutions of differing densities.

METHOD OF DENSITY DETERMINATIONS

Spring

F_w

F_b

Cage   Sample

Container
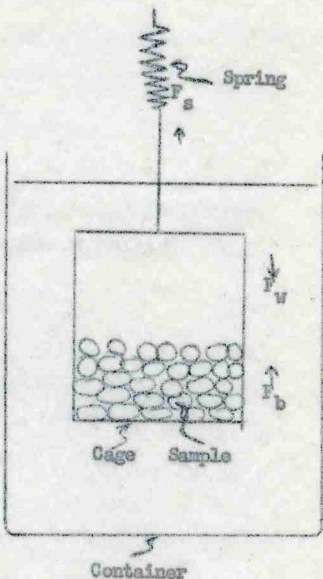
Fig. 1 Jolly Spring Balance   Fig. 2 Detail Sketch

The forces acting on a reference point of the cage support at water level are:

F_s = spring force = Kx (x is displacement difference in water before and after peanuts are added.)

F_w = weight of sample = mg

F_b = bouyancy effect = $\rho_w V_p$ g = $\rho_w \dfrac{m}{\rho_p}$ g

The weight in air of the sample can be determined using the spring:

F_w = mg = Kx' (x' is displacement difference in air before and after peanuts are added.)

For static equilibrium:

$$F_s + F_b = F_w$$

$$Kx + \frac{\rho_w Kx'}{\rho_P} = Kx'$$

$$\rho_P x + \rho_w x' = \rho_P x'$$

$$\rho_P = \frac{\rho_w x'}{x' - x}$$

Notice that it is not necessary that the spring constant be known. Also the gravitational constant does not have to be known.

TABLE 1. DENSITY MEASUREMENTS

Sample Number	Apparent Whole Kernel Density	Density of Separate Cotyledons
1B - 1	0.958	1.026
1B - 2	0.961	1.046
1B - 3	0.945	1.036
1B - 4	0.938	1.022
1B - 5	0.956	1.052
1A - 1	1.047	1.097
1A - 2	1.049	1.092
1A - 3	1.048	1.093
1A - 4	1.040	1.096
1A - 5	1.034	1.106

Mean values and standard deviations:

1B Cured at 125° F	$0.952 \pm .009$	$1.036 \pm .009$
1A Cured at room temperature	$1.044 \pm .006$	$1.097 \pm .005$

Hardness Investigations

The loosely defined agglomeration of numerous physical characteristics called "hardness" has been said by workers in the field to be associated with peanuts cured at high temperatures (Teter; Bailey, Pickett, and Futral; Giles and Dickens.) It is claimed that peanuts cured at high temperatures are harder or more brittle than peanuts cured at lower temperatures. There has been little work to substantiate or disprove these claims. In fact there has been little work done on the hardness of any agricultural products.

The term "hardness" used in reference to peanuts has been a subjective indication of the ease with which a peanut kernel can be crushed with the fingers or with "harder" tools such as fingernails or teeth. Hence the "hardness" referred to is probably resistance to penetration or shear. An objective measurement of differences would entail measuring the force required to penetrate or shear the peanut kernel with a given tool under given conditions. The outer surface of the peanut kernel would be the first point of contact in any casual subjective test. Therefore, it was decided to investigate surface characteristics primarily and interior characteristics secondarily.

Metallurgy is blessed with numerous tests to determine hardness (resistance to indentation) of metals. Various devices have been devised to determine resistance to abrasion, scratching, or marring of metals, plastics, and surface finishes. Comparison tests determine which minerals can scratch which others (Moh's scale.)

Penetrometers measure penetration of probes of standard weight and conformation into dairy and petroleum products after elapsed times.

Some, although certainly not all, of the characteristics taken as measurements of "hardness" are:

1. Indentation or penetration under load.
2. Indentation or penetration after release of load.
3. Instantaneous return of the energy of indentation indicative of perfectly elastic solid.
4. Resistance to shear.
5. Resistance to scratch.
6. Resistance to abrasion.
7. Brittleness or resistance to fracture.

Obviously then, there would be two distinct reasons for undertaking hardness investigation. First, it has been claimed (without adequate verification) that peanuts cured at high temperatures are "harder" than peanuts cured at lower temperatures. These claims could be verified or disproved and the measurements could possibly be developed into a reasonable determination of curing temperature. Second, hardness investigations would be basic research into an area in which little work has been done with respect to agricultural products and in which knowledge, both theoretical and applied, is sparce. For these reasons this area has been actively pursued by the writer.

In any of the hardness characteristics previously listed, a primary parameter is the force used or required. A commercially available instrument, the Instron Tester can accurately and precisely measure forces over a wide range when testing materials for tensile strength. It can be adapted to compressive testing by use of accessory parts. The writer has designed and built accessory parts to use an Instron Tester to measure compressive forces by preloading an available tension measur-

ing cell which measures forces within the required range of values.

Figure 3. Punch Holder and Plate for Instron Tester

Preliminary tests have been run in the following manner: single
cotyledons have been placed, flat surface down, on a plate under a
cylindrical flat ended probe of about one-sixteenth inch diameter.
The plate ascends at a fixed velocity and the force required to push
the probe through the cotyledon and into a matching hole in the plate
is recorded. These graphs of force versus displacement have been
analyzed for a number of kernel havles cured at two temperatures.
Sample measurements are included. Although significant differences
may be indicated it must be remembered that these are preliminary tests
only with an insufficient number of samples. Further modifications of
equipment and technique are planned to eliminate undesired variables
and to test peanut cotyledons over a wide range of curing treatments.
Tests are planned to determine the effect of moisture content on hardness.

A typical curve of punch displacement versus punch force
might look like the following given in Fig. 4:
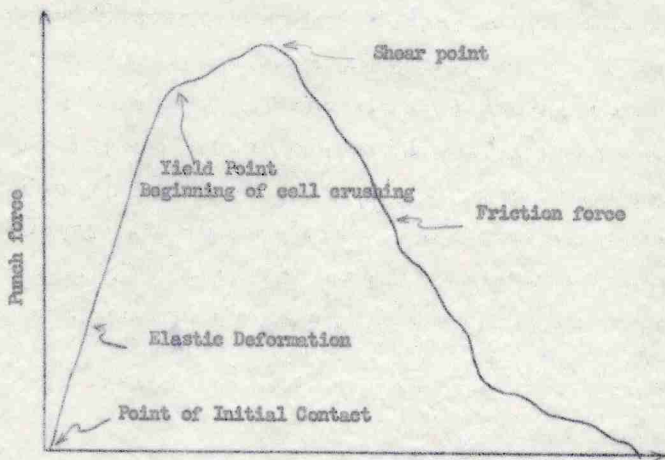
Figure 4

These tests are analogous to press mounted punch and die
equipment used in manufacturing processes. Like them the punch
has three stages of action: elastic deformation, plastic deformation
or penetration, and shear. The force versus displacement chart
might easily give measurements therefore of the elastic yield point,
shear modulus, energy requirements, or other parameters. These
measurements would be indicative of surface and internal qualities
which could indicate differences between curing treatments based on
physical or structural differences.

TABLE 2. HARDNESS TESTS USING ONE—SIXTEENTH
INCH PROBE

	Cotyledons Cured at 70° F				Cotyledons Cured at 125° F	
Sample	Maximum Force Required Dynes	Energy Required Ergs		Sample	Maximum Force Required Dynes	Energy Required Ergs
1	1240	363		1	1160	279
2	1110	331		2	1230	329
3	1360	305		3	1610	261
4	1620	462		4	1480	255
5	1260	417		5	1420	325
6	1300	323		6	1150	283
7	1430	335		7	1040	188
8	1870	503		8	1580	329
9	1770	420		9	1430	481
10	1150	365		10	1250	313
11	1250	322		11	1140	241
12	1420	438		12	1260	314
13	1640	356				
14	1390	477				
15	1280	482				
16	1100	258				
17	1620	487				
18	1480	427				

Mean Forces, Energies, and Standard Deviations

75°	1405 + 50.2 dynes
125°	1313 ∓ 57.2 dynes
75°	392.8 + 17.2 ergs
125°	299.8 ∓ 20.5 ergs

LITERATURE CITED

Bailey, W. K., T. A. Pickett, and J. G. Futral. 1954. Rapid
    Curing Adversely Affects Quality of Peanuts. Peanut Journal
    and Nut World. 33: 17.

Giles, G. W., and J. W. Dickens. 1958. Improving the Curing Operation
    in Peanut Production. Peanut Journal and Nut World
    38: 11, 25-29.

Pickett, T. A., and K. T. Holley. 1957. Shrinkage in Curing
    Peanuts. Peanut Journal and Nut World. 36: 13-15.

Teter, N. C. 1957. Physical and Pathological Factors Affecting
    Quality of Peanuts as Influenced by Curing. Proceedings -
    Peanut Research Conference. 54-62.

FLOW OF WATER THROUGH UNSATURATED FLOW

In drainage as in irrigation, one is concerned with characterizing the rate of flow of water through soil and the moisture content and energy status of the water at any point and time. Since a large portion of the water moves through unsaturated regions and, furthermore, these unsaturated regions are of primary importance in plant growth, it is of great importance to be able to describe these unsaturated flow processes quantitatively.

This flow phenomenon may be described by the equation

$$\nabla \cdot K \nabla \phi = \partial \theta / \partial t,$$

where ϕ represents the total moisture potential and θ the volumetric moisture content. The conductivity K is not a constant, but a variable dependent on the moisture status. We choose to state $K = K(\phi)$. Considering the difficulty of obtaining analytic solutions to this equation for meaningful boundary conditions, solutions by iterative techniques are being sought.

In preliminary investigations, five geometries of tile drainage systems with different boundary conditions were programmed for and solved on the Univac 1105, using Southwell iteration techniques. With a 7 x 9 mesh (63 grid points) convergence was attained in approximately 30 seconds. A similar flow problem with a 20 x 40 mesh had not converged satisfactorily after 6 minutes.

Present work is directed towards developing methods of solution with faster rates of convergence and developing means of evaluating the error. Error evaluation is of prime importance. An apparently rigorous mathematical technique employing matrix methods has been devised for estimating maximum error, but this technique has not been tested on a digital computer.

Present estimates suggest that a 10 x 10 mesh could be traversed 100 times in 3 minutes on a millisecond machine. Theory indicates that the maximum error should approach zero after that number of iterations. By partitioning the matrices, problems with finer meshes could be solved. Such refinement is necessary for useful answers.

The work is carried on under Exp. Sta. Project S-224 by John I. Sewell under the direction of Jan van Schilfgaarde.

SUPPLY AND NEED OF IRRIGATION WATER

Research in irrigation is currently being directed towards an analysis of water supply and needs by use of climatological data. Some analyses have been made in the past of the frequency of occurrence of drought days and of need for irrigation, using the following basic equation:

$$SMC_f = SMC_i + P - ET - Ex.$$

The final soil moisture content (SMC_f) is determined from the initial (SMC_i) for each day by the addition of the amount of precipitation (P) and the subtraction of the evapotranspiration (ET) and excess (Ex). Refined methods of computation of ET, based on a better approximation of soil moisture distribution, have since been developed.

It is desirable to make a new, more comprehensive analysis of the daily moisture balance to evaluate the frequency of occurrence of runoff and irrigation requirements.

In this connection, the following points are noted:

(1) For purposes of prediction, we need to analyze at least 25 years of back records.

(2) The water balance procedure on which the analysis is based requires daily input and computation.

(3) To characterize conditions throughout the Piedmont and Coastal Plain, records from 20-30 weather stations must be processed.

(4) In relation to the planting of a variety of crops on a variety of soils, a range of parameters must be used.

(5) A relatively compact output is desirable.

These observations indicate that:

(a) High-speed digital computation facilities are a necessity.

(b) A large amount of input data handling is required.

(c) A relatively large memory storage capacity is necessary.

Specifically, this work requires a medium size computer with high speed at least in simple arithmetic operations and high-speed input (preferably magnetic tape). If magnetic tape input were available, card-to-tape conversion would be desirable, since the data are already available on cards. Time required for computation would be about 20 hours on a machine such as the Univac 1105.

The above work is carried on as part of Exp. Sta. Project S-224, by E. H. Wiser under the direction of Jan van Schilfgaarde.

Intermittent Recording with a Multipoint Instrument

K. A. Jordan and C. W. Suggs
Member ASAE   Member ASAE

THE problems involved in measuring variables simultaneously, as required in environmental research investigations, for example, have led the authors to develop techniques for recording several environmental variables with a multipoint instrument at prescribed time intervals. Circuits are developed, using a rational method, for controlling the chart and printing-drive mechanism in order to print, at a maximum rate, one set of points followed by an adjustable off time. The advantages of the system are: (1) all variables are recorded on one chart; (2) variables can be recorded in rapid succession, limited only by the recorder balancing speed; (3) data can be spaced for readability (high chart speed can be used), (4) data during critical periods can be collected more frequently; the time between sets of data can be easily adjusted, and (5) chart length and cost are minimized; data are collected only at desired times.

Intermittent Operation

Where several measurements are taken which will be used to calculate other quantities, it is desirable to have

these measurements recorded simultaneously. As an example of this, black-globe temperature must be used with air velocity to calculate mean-radiant temperature. Many multipoint recorders have switching speeds of four seconds and less. For many situations this may be considered simultaneous. When fast printing speeds are used, however, the chart speed must also be fast in order that one point will not be printed over another point, making the record difficult to decode. The requirements for fast-printing speeds and fast-chart speeds are usually tempered by the cost of chart paper and the difficulty of handling great lengths of charts. If the chart-print-drive motor were turned off, after printing one set of points at the maximum rate, the cost and length of chart would be greatly reduced. The time desired between each set of points is determined by the nature of the application. It may be desired to record the initial portions with a different interval from later portions, as might be required in drying experiments.

Circuit Description

A multipoint recorder was used which had the chart and printing mechanisms directly connected. A microswitch was mounted within the recorder so that it was actuated by a pin on the printing mechanism shaft when one set of points was recorded. An interval timer (Industrial Timer Corp. Model TDAF-60M) with a clutch-driven cam arm actuated another microswitch. These switches were connected essentially as shown in Fig. 1 in order to energize the chart-print motor at the desired times.

The chart-print-drive switching sequence is discussed
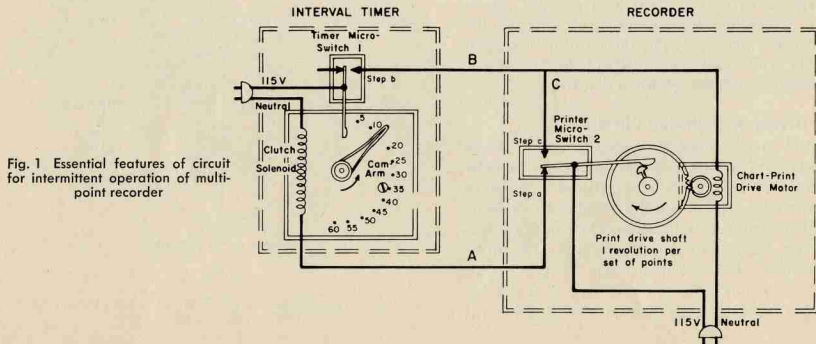
Fig. 1 Essential features of circuit for intermittent operation of multipoint recorder

below, starting between the printing cycles with each step lettered as in Sequence Table 1.

SEQUENCE TABLE 1

	Steps	Elements			
		Timer switch 1	Printer switch 2	Chart-print drive motor	Typical time, minutes
(a)	Clutch engaged timing between print cycles	Not actuated	Actuated	Off	30
(b)	End of timing; start printing	Actuated	Actuated		0.2
(c)	After printing several points	Actuated	Not actuated		0.01
(d)	Clutch disengaged	Not actuated	Not actuated		1
(a)	End of print cycle; engage clutch	(Return to original conditions)			

(a) The clutch-driven cam arm is sweeping through an arc timing the off period. The lever on timer switch 1 is actuated by this cam arm; therefore during this time the cam arm switch 1 is *not actuated*. The chart-print-drive *motor* is *off*. The lever of printer switch 2 which is resting on a pin in the printing drive shaft is actuated but the shaft is not turning. (All elements in Fig. 1 are shown in the condition described in step *(a)*. Circuit A is completed energizing the interval-timer clutch solenoid.

(b) At the end of the timing cycle the cam arm *actuates* timer switch 1. This completes circuit B and the chart-print drive *motor* is turned *on*. The printer switch 2 remains *actuated* for about 0.2 min after the printing drive shaft starts turning.

(c) When the printer switch 2 lever falls off the pin on the printing drive shaft, it is *not actuated* which completes circuit C through the contacts of switch 2. Chart-print drive *motor* remains *on*. Timer switch 1 remains *actuated* for about 0.01 min since printer switch 2 is snap action.

(d) Timer switch 1 is *not actuated* when the cam arm resets. Switch 2 remains *not actuated* as in step *(c)* which has caused the solenoid to release the cam arm. The chart-print drive *motor* remains *on* for about a minute while all the points are being recorded on the chart.

(e) After a set of points has been recorded printer switch 2 is *actuated* which interrupts circuit C turning the chart-print drive *motor off*. The timer clutch is engaged when circuit A is again completed and the cam arm is driven through the position shown in Fig. 1.

Rational Design of Switching Circuits

A control circuit can easily be visualized when only a few elements are involved, but as the circuit becomes more complicated, a great deal of experience is needed to perfect a control system. Rational procedures are available for designing electric control systems. These design procedures are best mastered upon single circuits which can be easily visualized. The first design step — which has already been done for the chart-print motor — is to develop a sequence table. Then a pie diagram is constructed as is

shown in Figure 2. The pie is divided in half. One half represents one switch in the actuated position and the other half represents the same switch in the "normal" or not actuated position. Each switch is assigned two areas shown in the Figs. 2.1 and 2.2 and the two areas assigned each switch must completely cover the pie. The pie diagrams are superimposed where each quarter represents one of the four possible combinations of switch positions. The wedge associated with each combination of switch positions has been established by the area assignments and is lettered at the apex of the wedge in Fig. 2.3. Then the condition of the motor (on or off) is placed in each wedge corresponding to the step associated with that wedge.

The circuit with the fewest switch contacts is obtained by properly combining the wedges in order that one contact can satisfy several steps. Each step taken by itself requires two contacts; that is, wedge c requires that switch 2 is not actuated and that switch 1 is actuated. If wedges b and c are considered together, the switching requirements can be satisfied with one contact on switch 1. The proper combinations of wedges are shown by the dotted lines in Fig. 2.3.

Translating this pie diagram into an electrical circuit, each combination of wedges will result in a parallel circuit. The combinations shown by the dotted lines will result in two parallel circuits either of which will energize the chart-print drive motor during the desired print cycle. These parallel branches will cause the chart-print motor to be on when either switch 1 is actuated (wedges b and c) or switch 2 is not actuated (wedges c and d). In order for the chart-print motor to be energized when switch 2 is not actuated, a normally closed contact on switch 2 must be utilized. The circuit for the chart-print
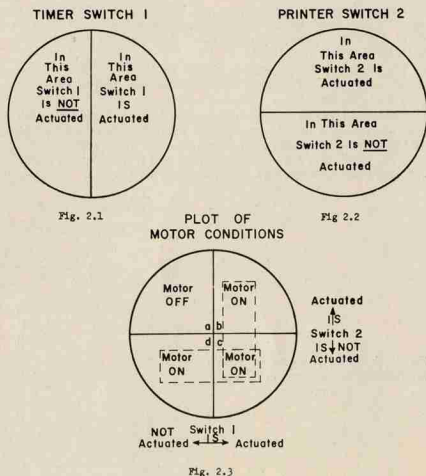
Fig. 2 Pie diagram representation of switch positions for energizing the chart-print motor
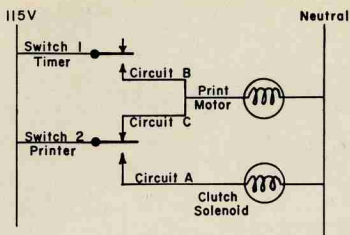
Fig. 3 Line diagram of circuit

motor and the clutch solenoid are presented with a line diagram in Fig. 3.

Further developments in the rational design of switching circuits are presented in numerous texts. The text most useful to the authors was "Applied Boolean Algebra" by Franz E. Hohn.

Conclusion

It is possible to record with one multipoint instrument environmental variables almost simultaneously at definite intervals of time over an extended period without the expense or inconvenience of great lengths of chart paper. The design of switching circuits is indicated which should be most useful for the inexperienced since rational procedures are followed. The utility of this approach is more dramatic as the switching system becomes more involved.

• •
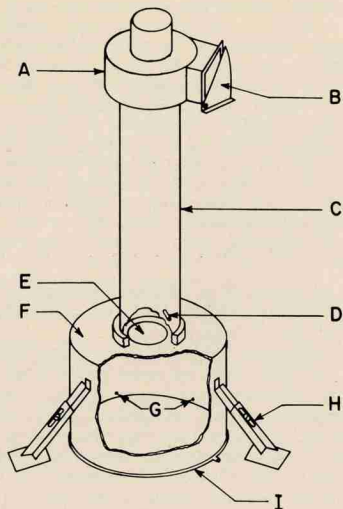
Fig. 1 Schematic drawing of air flow meter: A, fan (1/40 hp, 100 cfm); B, adjustable damper; C, thin-walled tubing, 4 to 5 in. I.D., four diameters long; D, pressure tap 0.4 orifice diameters, downstream from orifice; E, orifice, 3.34 in. diameter; F, cylinder, 13.54 in. diameter, 8 in. high; G, pin holes connecting piezometer ring to inside of cylinder wall; H, adjustable supports for flotation; I, piezometer ring, ¼-in. copper tubing

Device Measures Air Flow

Through Porous Surfaces

E. O. Beasley
Member ASAE
and
J. W. Dickens
Member ASAE

THE methods available for measuring flow rates of air through agricultural commodities and other materials, which are being dried or aerated with forced air, have not been completely satisfactory in all situations. One of the simplest and most widely used methods, which requires a minimum investment in equipment, consists of measuring the decrease in static pressure of the air as a result of its movement through a layer of the commodity. The air-flow rate corresponding to this static-pressure decrease is obtained from a graph or table, which is available for most agricultural crops (1)*. This method has the following disadvantages: *(a)* characteristic curves must be developed for each commodity; *(b)* unless the composition of the commodity exactly matches the material used in developing the curve, the measurement will not be accurate, and *(c)* only the average velocity through the layer is determined, since variations in the air-flow pattern due to non-homogeneity of the layer cannot be detected.

Various types of anemometers are available which permit a more direct measurement of air velocity, but they are relatively expensive and delicate for field use. This paper reports the development of a device for making direct field measurements of air flow through a porous surface.

Design and Construction

The design objectives for the device were: *(a)* to measure the quantity of air emerging from a small section

Fig. 2 Experimental device for measuring air-flow rate

*Numbers in parentheses refer to the appended references.
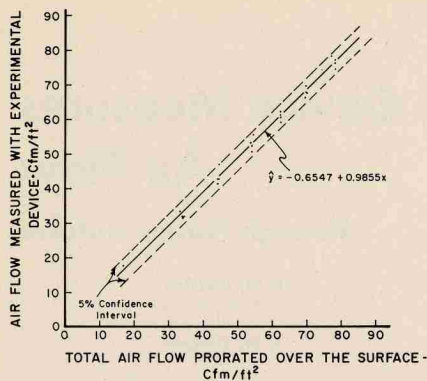
Fig. 3 Measured air flow calibrated against total
air flow prorated over the surface

of any porous surface, such as that formed by grain and
seeds, without causing a disturbance in the air-flow pat-
tern which would affect the measurement; *(b)* to make
the device as simple, rugged, and direct-reading as pos-
sible, and *(c)* to obtain an accuracy of measurement suit-
able for general field use.

The principle employed was to entrap the air flowing
through a known surface area in the open end of a cyl-
inder placed over the area and to discharge the air
through an orifice in the other end of the cylinder for
quantitative measurement. In order to overcome the re-
sistance to flow which the orifice introduced, causing
some air to be diverted around the cylinder, a fan with
adjustable damper was mounted downstream from the
orifice.

A drawing of the measuring device is shown in Fig. 1.
The orifice (E) is centrally located in the end plate (F)
of a sheet metal cylinder whose lower end rests on the
surface of the material being aerated. A pipe of suitable
diameter and length connects the orifice to the intake of
the fan (2). A piezometer ring (I) fitted around the out-
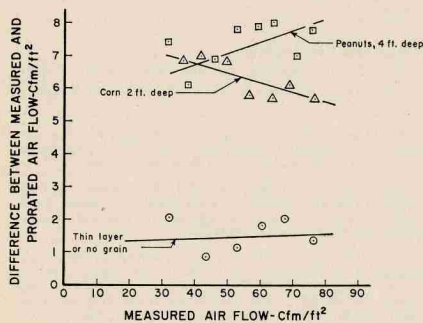
Fig. 4 Difference between measured and prorated
air flow at various depths of grain

side of the cylinder, adjacent to the open end, has several
small holes drilled through from the ring to the inside
surface of the cylinder.

In operation the device is set on the surface of the
grain or other material, through which air is moving up-
ward, as in Fig. 2. Adjustable feet support enough of
the weight to keep the leading edge of the cylinder from
sinking below the surface. The damper on the fan is ad-
justed until zero static air-pressure difference exists be-
tween the surface of the grain just outside the cylinder
wall and just inside, as indicated by a differential mi-
cromanometer. The suction tube of the micromanometer
is then connected to the pressure tap on the pipe down-
stream from the orifice, and the static-pressure drop across
the orifice is read. The quantity of air flowing through
the orifice is given by the relation (2):

$$Q = 1096.5\ CA\sqrt{P/\rho} \quad \ldots \ldots \ldots \quad [1]$$

where

Q = quantity of air, cubic feet per minute
C = orifice coefficient (0.601 for intake orifice)
A = area of orifice, square feet
P = pressure drop across orifice, inches of water
ρ = density of the air, pounds per cubic foot

Since the surface area covered by the cylinder is known,
the average air velocity can be calculated. Orifice calibra-
tion curves constructed from the above equation, for
densities in the range normally encountered, provide a
quick and convenient means of determining the air flow.

Adjusting the static pressure at the surface of the
grain under the cylinder to equal that at the surface out-
side the cylinder insures that the pattern of air movement
up through the layer of grain will not be disturbed by the
presence of the measuring device.

Test Results

Formula [1] applies to an intake orifice with a room
or plenum approach. It was desirable to keep the dimen-
sions of the cylinder as small as possible for compactness
and portability, and still approximate with sufficient ac-
curacy a plenum approach to the orifice. The first cylinder,
which was 14 in. high and 18 in. in diameter, was re-
placed by one 8 in. high and 13.54 in. in diameter, with
no apparent decrease in the accuracy of measurement. The
smaller dimensions were therefore used for all subsequent
measurements.

As a means of evaluating the performance of the
device, a test chamber was built which provided air flows
of variable magnitude. A high-pressure fan with ad-
justable damper drew in air through a 4-in. orifice
mounted at the end of a 6-in. pipe, and discharged it
into a 4-ft square plenum underneath a wire-mesh floor.
Two burlap stilling screens were mounted 4 in. apart
underneath the floor, and four layers of burlap were
placed on top of the floor. These screens distributed the
air uniformly over the floor surface. The total air volume
drawn in through the orifice was measured and prorated
over the floor area, to provide a standard against which
the experimental device could be compared.

Data were obtained with the cylinder resting directly
on the burlap-covered wire floor, suspended one and one-
half inches above the floor, and resting on one-inch layers

of shelled corn and unshelled peanuts spread over the floor on top of the burlap. The air flows measured under these four conditions and the corresponding prorated air flows were used to construct the line of Fig. 3 and to determine the five percent confidence interval about the line.

Additional measurements were made with the device resting on 2-ft layers of shelled corn and 4-ft layers of unshelled peanuts. Greater differences were observed between measured and prorated air flows through these thick layers of grain than through very thin layers, as shown in Fig. 4. Due to the tendency for more air to flow next to the wall of the box where resistance is lower, the total air flow is not uniformly distributed over the surface of thick layers; therefore, the prorated values are high and the measured values reflect the actual amount of air passing through the grain layer directly beneath the measuring device. Data obtained from thick layers were not included in the performance evaluation of Fig. 3.

The range of air flows which can be measured is dependent upon the size of orifice used. Static pressure differential across the orifice should be at least 0.10 in. for the smallest air flow to be measured, and probably should not exceed 2.0 in. for the maximum rate of air flow. Accuracy is limited both by the precision with which static-pressure differences across the cylinder wall can be eliminated, and by the accuracy of the measurement of the pressure drop across the orifice.

Summary and Conclusions

A device was designed and tested which is sturdy, simple to operate, and enables a direct measurement of air flow through a small surface area. The primary element of the apparatus is an intake orifice, through which air emerging from a known area of porous surface is directed. The impedance of the orifice to normal air flow is offset by an adjustable fan whose intake is connected to the orifice. Adjustment of the fan to the proper rate of discharge is accomplished by equalizing the static pressure at the surface of the grain under the apparatus with that at the surface outside but adjacent to the apparatus. A differential micromanometer is used for this adjustment, and to subsequently read the pressure drop across the orifice.

Accuracy was generally within three percent of the largest air flow measured. Errors due to edge effect and trash deposits, which are inherent in indirect air-flow measurements, are not incurred with this method. The apparatus can be used on a wide variety of commodities, because its operation is not dependent on the medium through which air is flowing.

References

1 Shedd, C. K. Resistance of grains and seeds to air flow. AGRICULTURAL ENGINEERING 34:(9), September 1953.

2 Madison, Richard D. (Ed.) Fan Engineering. Buffalo Forge Co., Buffalo, N.Y., 1949. ● ●

Theoretical Implications of Electrical Fields on Deposition of Charged Particles

H. D. Bowen, W. E. Splinter, and W. M. Carleton

ASSOC. MEMBER ASAE   MEMBER ASAE   MEMBER ASAE

THE principles of electrostatics have been successfully exploited by industry to improve substantially the efficiency of such seemingly diverse processes as flyash and fume removal from industrial smokestacks, paint spraying, and smoke curing of fish. Closer examination reveals that all of these industrial processes have in common the same two general objectives: to remove small particles from a gas and to deposit them on a surface.

The problem of the application of pesticides to plant surfaces in the form of sprays, dusts and smokes has the same general objectives as the industrial processes just referred to. However, there are several important differences in industrial and agricultural conditions that prevents direct transfer of the technology from the factory to the field. The more important of these differences are (a) that the range of environment encountered in the agricultural field is much greater than in the factory; (b) that agricultural field equipment must be more mobile and relatively lower in cost than industrial equipment, and (c) that multiple hidden surfaces requiring treatment are shielded in a very complex way, whereas exposed surfaces are the more important ones in the industrial situations described.

Laboratory studies at Michigan State University and North Carolina State College have repeatedly shown that under favorable conditions charging dusts increases deposits from 4 to 1 to 10 to 1 over uncharged dusts. Field studies have generally shown a 2 to 1 ratio of deposit in favor of charging dusts (2, 4, 7, 13)°. There have been some notable failures especially at the extremes of the relative humidity range encountered in the field (4, 5).

In view of the large improvements in deposition that can be obtained under ideal environmental conditions and the economic success of electrostatic methods in industrial processes, a detailed investigation of those aspects of
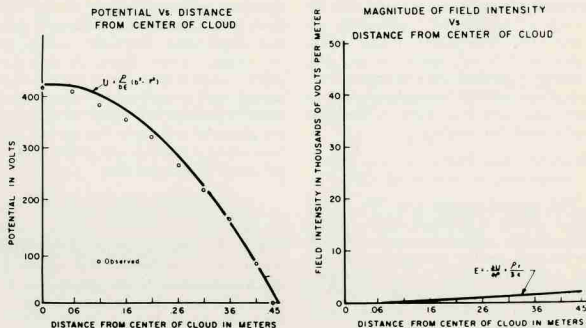
FIG. 1(a) (Left) Comparison of theoretical curve and empirical observations of the electric potential distribution of a spherical cloud of charged particles with a charge density of 1.113×10^{-7} coulombs per meter.[a] The outer boundary of the cloud is suppressed to zero potential ● FIG. 1(b) (Right) Electric field intensity distribution of the cloud whose potential distribution shows in Fig. 1(a). The field intensity is positive and the force on a particle of the cloud would be directed away from the center.

the process that directly contribute to the enlargement of the range of environmental and other conditions, for which the full benefit from charging can be reliably expected, is warranted.

An understanding of the effective use of electrostatic principles for increasing the deposition efficiency of agricultural dusts, sprays, and smokes demands consideration of two operations: electrical charging of pesticide particles into a unsigned cloud and the establishment and maintenance of a significant electrical deposition field.

A discussion of the methods for charging particles and the problems involved in attaining adequate charging is reserved for a later paper. The ionized field method (2) was used in charging the particles for the tests relating to this paper.

The electrical force supplements the inertial, gravitational and thermal forces developed in the application process. The total amount of the deposit is linearly related to the sum of all forces acting on the particles in the direction of the target, assuming no erosion losses. However, the charging of the particles is a necessary but not a sufficient condition for the establishment of an adequate electrical force field for a significant increase in particle deposition due to charging. This paper deals with some of the theoretical aspects of the electrical field E, as it is influenced by the configuration of the

system, factors that promote or inhibit an induced charge on the target surface, and the charge density of the dust cloud.

Once the individual particles have been charged they form, in the aggregate, a charged cloud of a single electrical sign, and are therefore subjected to electrical forces.

In the absence of appreciable magnetic fluxes, the force on a single particle is given by

$$F = neE = qE = -q\,\frac{\partial U}{\partial X_i}$$

Where n is the number of elementary electron charges e on the particle and q is the total charge ne on the particle, $E = -\partial U/\partial X_i$, the field intensity or negative of the potential gradient along a generalized coordinate X_i.

Plant surfaces that would normally be of interest for coating with pesticides can be loosely classified as having parts that are either a spherical, cylindrical, or planar configuration corresponding roughly to the shapes of fruits, stems and leaves, respectively. All three of these configurations can be completely described mathematically when one or more of the boundaries are infinite; however, only the spherical configuration allows a complete mathematical description when all of the boundaries are finite.

Clouds with spherical boundaries and with approximately uniform charge

density were easily produced experimentally. However, clouds with cylindrical and planar boundaries could not be produced with satisfactory uniformity of charge distribution with the facilities available.

Since the spherical cloud could be both mathematically described and experimentally produced, a study of it allowed a satisfactory verification of theory by observation. Planar fields which could be calculated but not satisfactorily measured were linked to empirical observation through similarities with the spherical field. Cylindrical fields were not studied.

EQUATION FOR POTENTIAL AND FIELD INTENSITY OF SPHERICAL CLOUD

The general equation for the potential U within a spherical cloud of uniform charge density ρ and radius b enclosing a smaller concentric conducting sphere of radius a was developed by Bowen (3) for the case where the outer boundary of the cloud b was suppressed to zero.

The following equation is in the MKS system:

$$U = \frac{\rho}{6\epsilon}(b^2 - r^2) + \frac{\rho a^3}{3\epsilon}\left\{\frac{1}{b} - \frac{1}{r}\right\} - \frac{Va}{r} + \frac{Va}{b} \dots a \le r \le b \dots [1]$$

r is the radial position coordinate and ϵ is the absolute dielectric constant of the medium. V is a fictitious voltage arising from the charge, $-Q = -V4\pi \epsilon a$, required to maintain the conducting sphere at any specified voltage V' in the presence of the cloud. Within the sphere the potential $U = V'$. The electric field intensity E is given by

$$E = -\frac{\partial U}{\partial r} = \frac{\rho r}{3\epsilon} - \frac{\rho a^3}{3\epsilon r^2} - \frac{Va}{r^2}$$
$$\dots a < r < b \;[2]$$

$$E = -\frac{V}{2a} \dots r = a \;[2a]$$

$$E = \frac{\rho b}{3\epsilon} - \frac{\rho a^3}{3\epsilon b^2} - \frac{Va}{b^2}$$
$$\dots r = b \;[2b]$$

(A brief development of the equation is given in the appendix.)

MEASUREMENT OF POTENTIAL DISTRIBUTION OF SPHERICAL DUST CLOUD WITH UNIFORM CHARGE DENSITY

The approach to measurement of potential distribution was that of keeping a turbulent and uniformly dispersed cloud of charged dust particles circulating rapidly through the volume to be measured. The charge density was maintained at a low level, so that the dust that precipitated out was only a minor part of the dust that was circulated through the system.

A spherically shaped cloud of dust was created by filling the chamber with a dust cloud and electrically grounding a spherical wire mesh cage suspended from the ceiling of the chamber. The mesh of the cage was large enough so that free circulation of charged dust occurred throughout the chamber including the spherical volume within the wire mesh cage. A fixed probe with radioactive polonium nitrate on its surface and connected to a calibrated gold leaf electroscope was used to monitor the charge density level. A movable probe coated with radioactive polonium nitrate and connected to an electrostatic voltmeter was used to measure the potential voltage at the various stations along a vertical axis of the spherical cloud of charged dust.

EMPIRICAL VS CALCULATED POTENTIAL DISTRIBUTION

Several potential distributions were measured and compared with appropriate modifications of the general equation. The two distributions shown in Figs. 1a and 2a serve to typify the results of these tests.

A study of the observed potential distribution versus the calculated potential distribution, indicates that a completely uniform charge density was not achieved, there being a lower density in the interior parts and slightly increased density nearer the outer boundary of all tests. However, there is no doubt but that the observed potential distribution satisfactorily verified the equations. By the substitution of the appropriate boundary condition the general equation may be modified to include the case where (a) there is no charge on the enclosed sphere; (b) there is no matter within the cloud; (c) there is no outer conducting boundary; (d) there is an arbitrary positive or negative value of the voltage on the enclosed sphere and the outer boundary.

PARTICULAR EQUATIONS OF UNIFORM CHARGED CLOUDS WITH SPHERICAL CONFIGURATIONS

Charged Spherical Cloud with Boundary at Zero Potential

For the most general case, if a thin conducting spherical shell of radius b were in some manner filled with a uniform density of charged particles and the conducting shell was connected to ground, a charged spherical cloud with boundary at zero potential would result.

Since a is zero in equation [1], the potential is given by

$$U = \frac{\rho}{6\epsilon}(b^2 - r^2) \dots r \le b \;[3]$$

and the electric field intensity is given by

$$E = -\frac{\partial U}{\partial r} = \frac{\rho r}{3\epsilon} \dots r < b \;[4]$$

$$E = \frac{\rho b}{3\epsilon} \dots r = b \;[4a]$$

The maximum potential occurs at the center of the cloud, and all particles of the cloud (except at the very center) are forced toward the outer boundary.

The potential and field intensity distributions for $\rho = 1.113 \times 10^{-7}$ coulombs per meter^3 $\epsilon = 8.854 \times 10^{-12}$ farads per meter, $a = 0.01$ meter, and $b = 0.45$ meter are shown in Figs. 1(a) and 1(b), respectively.

Charged Spherical Cloud with Inner Boundary Floating and Outer Boundary At Zero Potential

A charged, hollow spherical cloud may be visualized as the one that would be formed if an uncharged sphere were inserted into the center of a spherical cloud of charged particles. The cloud boundary next to the sphere (inner boundary of the cloud) would be free of unbound charges and the potential of the sphere and the cloud-sphere boundary would be free to float. This would be simulated by a single kernel of wheat or corn falling through a cloud of charged dust. The cloud-sphere boundary potential would then be determined by charges other than those on the boundary itself and would change in magnitude if any charges on neighboring boundaries or in the surrounding space changed in magnitude or position. If the shell were electrically connected to earth, a hollow spherical charged cloud with inner boundary floating and outer boundary at zero potential would result.

The equation for the potential distribution can now be obtained from the general equation [1] by setting the fictitious voltage V equal to 0, and is

$$U = \frac{\rho}{6\epsilon}(b^2 - r^2) + \frac{\rho a^3}{3\epsilon}\left\{\frac{1}{b} - \frac{1}{r}\right\}$$
$$\dots a \le r \le b \;[5]$$

The field intensity is given by

$$E = -\frac{\partial U}{\partial r} = \frac{\rho r}{3\epsilon} - \frac{\rho a^3}{3\epsilon r^2}$$
$$\dots a < r < b \;[6]$$

The potential is a maximum and the field intensity is a minimum (zero) at the inner boundary of the cloud. The field intensity is zero both within and on the surface of the interior sphere. Therefore, electrical field forces will actually prevent the deposition of charged particles on the surface of the interior sphere even though the surface is conductive.

Charged, Hollow, Spherical Cloud with Inner and Outer Boundary at Zero Potential

If the uncharged sphere interior to the cloud is conductive and is electrically connected to ground, it roughly simulates a plant within a uniformly charged cloud.

The equation may be obtained from equation [1] by setting the surface potential of the sphere V' equal to zero. The value of the fictitious voltage $-V$, resulting from the induced charge $-Q_s$ on the sphere at zero potential is obtained by setting $V' = U = 0$, at $r = a$ and solving for V. The reader should recognize that V, the fictitious voltage, will be positive as solved from the equation and will be substituted back in the equation as a positive value. The negative sign is already accounted for in the equation.

The equation for this case is the general equation [1] and is repeated for convenience:

$$U = \frac{\rho}{6\epsilon}(b^2 - r^2) + \frac{\rho a^3}{3\epsilon}\left\{\frac{1}{b} - \frac{1}{r}\right\} - \frac{Va}{r} + \frac{Va}{b} \dots a \le r \le b \;[7]$$

The field intensity is given by equation [2] and is:

$$E = -\frac{\partial U}{\partial r} = \frac{\rho r}{3\epsilon} - \frac{\rho a^3}{3\epsilon r^2} - \frac{Va}{r^2}$$
$$\dots a \le r \le b \;[8]$$

A maximum of the cloud potential U_{max} occurs at $r = r_{Umax}$

$$r_{Umax} = \sqrt[3]{a^3 + (3\epsilon Va/\rho)} \dots [9]$$

meters as can be noted from Figs. 3a and 3b. The forces exerted on the particles of the cloud are directed toward the grounded sphere of radius a from $a \le r \le r_{Umax}$ and are directed toward the grounded outer boundary at radius b from $r_{Umax} \le r \le b$. At r_{Umax} the force on a particle of the cloud is zero. The field intensity E on the inner boundary of the cloud just off the sphere is $E = -V/a$ and the field intensity on the sphere surface at $r = a$, is $-V/2a$. The field intensity within the sphere at $O \le r < a$ is zero as can be noted from Fig. 3b. Deposition will be effected due to the presence of these electrical field forces.

Charged Hollow Spherical Cloud with Inner Boundary at Zero Potential and Outer Boundary Floating

If the conducting shell containing the cloud of charged particles was insulated from ground but the inner conducting sphere remained grounded, then the outer boundary would have a floating potential. This would simulate an instantaneous condition that results when a non-captive charged cloud first surrounds a grounded plant.
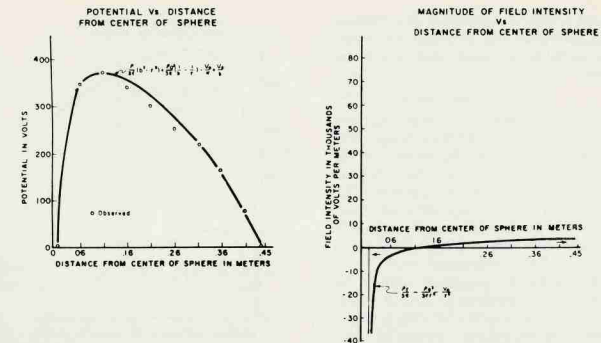
FIG. 2(a) (Left) Potential distribution along a radius of a hollow spherical cloud of uniform charge density with its inner and outer boundary at zero potential ● FIG. 2(b) (Right) Distribution along a radius of electric field intensity for the cloud with the potential distribution of Fig. 2(a).

The equation may be obtained from the general equation [1] by removing

$$-\frac{Va}{r} + \frac{Va}{b}$$

the two fields, $-U_{a+b}\big|_{r=b}$ and $+Va/b$, used to suppress the outer boundary to zero. The potential distribution is then given by:

$$U = \frac{\rho}{2\epsilon}\left\{b^2 - \frac{r^2}{3}\right\} - \frac{\rho a^3}{3\epsilon r} - \frac{Va}{r}$$
$$\dots a \le r \le b \;[10]$$

The field intensity E is given by:

$$E = -\frac{\partial U}{\partial r} = \frac{\rho r}{3\epsilon} - \frac{\rho a^3}{3\epsilon r^2} - \frac{Va}{r^2}$$
$$\dots a < r < b \;[11]$$

The form of equation [10] for the potential distribution of the cloud with the floating potential on the outer boundary is different from the form of the equation with the outer boundary at ground potential (equation [1]) because charges were removed from the outer boundary to make it a boundary of floating potential. However, the form of the field intensity is not changed from equation [2] since it is not an explicit function of the charges on the outer boundary at radius b.

The magnitudes of both the potentials and the field intensities in the cloud are increased, however, because the charge magnitude of the outer boundary at radius b influences the magnitude of the induced charge $-Q = -V4\pi\epsilon a$ on the surface of the sphere of radius a.

In the same manner as for the previous case, V may be found by solving equation [10] for V when $V' = U = 0$ at $r = a$. The negative charge $-Q_s$ induced on the sphere for the outer boundary at a floating potential is much greater in magnitude than when the outer boundary is at ground potential. Figs. 3a and 3b show a comparison of the potential and field intensity distributions for the same cloud with the outer boundary at ground potential and with the outer boundary at floating potential. ρ, a, b, and ϵ are the same as the previous cases. V is 436 volts when the outer boundary is grounded and is 1,275 volts when the outer boundary is free to float.

Field of Infinite Parallel Planes

The field of a uniform cloud sandwiched between two infinite parallel conducting planes at ground potential was developed by Splinter (13) and simulates the effect of a charged cloud between leaves, neglecting edge effects.

$$U = \frac{\rho}{2\epsilon}(dZ - Z^2) \dots 0 \le Z \le d$$

for the potential at any point between the planes where ρ is the charge density, d is the spacing, ϵ is the absolute dielectric constant of the medium and Z is the coordinate perpendicular to the planes. Fig. 4 shows the potential distribution and the field intensity as functions of distance along the Z axis.

The Field of Finite Planar Surfaces

A calculation of the potential and field intensity produced by a cylindrical cloud of equal length and diameter which simulates the effect of a charged cloud between actual leaves and the effect of a charged cloud next to an exterior leaf surface. The case for a single conducting boundary at ground potential and the case where the cylindrical cloud has both end boundaries at zero potential was developed by Bowen (3). Figs.

5 and 6 show the potential distributions and field-intensity distributions along the cylindrical cloud axes for these cases.

GENERAL DISCUSSION

There are several important concepts which may be gained from these theoretical models. A discussion of the practical implications of particle deposition as influenced by the electric fields depends upon a recognition of these concepts. In the following paragraphs the concepts and implications are first stated and then discussed.

A maximum potential occurs between two boundaries at ground potential. Uniform clouds of charged particles sandwiched between two grounded boundaries have a maximum potential which is centered between parallel planes or disks and which is closer to the inner boundary of a spherical cloud. The particles of the cloud are attracted to the grounded boundaries as in Figs. 1, 2, 3, 4, 5, and 6.

Greater potentials and field intensities are associated with a single grounded boundary than with two boundaries. When a cloud is bounded on one side by a grounded surface and on the other side by a floating boundary, the potential throughout the cloud and the field intensity next to the grounded surface are greater than when the cloud is bounded by two grounded surfaces. Consequently the outside surfaces of plants which are exposed to clouds with a single grounded boundary have higher field intensities and receive greater deposits than do inner surfaces of the plants where the clouds are sandwiched between two grounded boundaries.

The electric field strength is linearly related to the spacing of the grounded surfaces. The electric field strength is linearly related to the spacing of the leaves in the inner regions of the plant. This is most easily seen by examining the equation for the field intensity between parallel infinite planes at zero potential. There the field intensity is given by $E = \frac{\rho Z}{\epsilon} - \frac{\rho d}{2\epsilon}$. At the boundary where $Z = 0$, $E = -\frac{\rho d}{2\epsilon}$, which is a linear function of the spacing of the boundaries or the thickness of the cloud. Just off the surfaces of parallel disks with 4-in. diameter and 4-in. spacing, the electric field intensities are approximately 40 percent of those just off the surfaces of infinite planes with the same spacing. Closer spacing of the disks or leaves relative to their diameter will make their fields more closely approximate those of parallel infinite planes. Two grounded parallel leaves immersed in a charged cloud could conceivably have a somewhat higher field between them than would be available for a cloud sandwiched between two parallel planes that were grounded, because of edge effects. However, between leaves of plants with thick foliage it would appear that the magnitude of the field intensity would approximate that for parallel planes of equal spacing as the leaves.
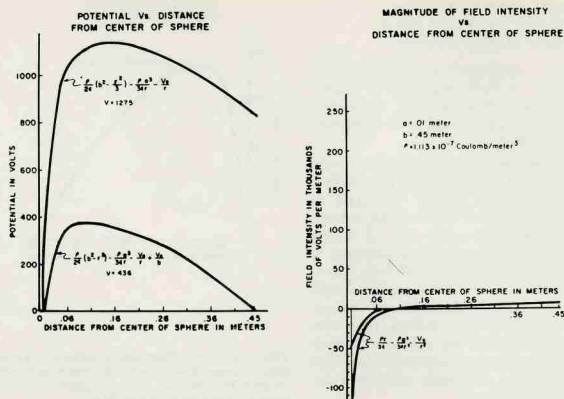
Under field conditions, the electric field intensities next to smooth leaf surfaces are estimated to have a magnitude of approximately 4.5×10^4 volts per meter in the inner regions of large plants such as cotton, assuming a leaf spacing of $d = 0.1$ meter, a charge density of $\rho = 0.8 \times 10^{-5}$ coulombs per meter[3], and the permittivity of free space $\epsilon = 8.854 \times 10^{-12}$ farads per meter.

Corona breakdown of the electric field is not a serious problem. The electric field intensity for the initiation of a corona discharge is approximately 3×10^6 volts per meter (1). A corona discharge is a breakdown of the dielectric properties of the air when an excessive electric field exists. In the region where the discharge takes place, a plasma of positive and negative ions are formed which would be expected to neutralize the charge on the particles in the corona region. The ratio of the electric field intensity causing corona discharge to the estimated electric field intensities next to leaves in the field is so large (67:1) that little difficulty from corona discharge on smooth leaves would be expected. A sharp point on a charged conductor has a high surface-charge density which produces a very intense electric field just off the surface in the dielectric even though the general field next to smooth surfaces is moderate (1). Leaf edges and leaf hairs have small radii. Corona discharges have been observed off the edges of celery leaves close to the nozzles of a duster where the dust cloud was highly concentrated. To what degree this corona discharge reduces deposition has not been ascertained but from the increased deposits that occur when the nozzles are placed close to plant surfaces, it is highly probable that charge densities of at least ten times those presently attainable could be safely used without serious problems from corona discharge neutralization.

A large waste occurs when clouds of charged dust are blown over the tops of plants. Since a maximum potential occurs in a cloud with only one boundary grounded, it is obvious that only a fraction of the cloud is driven to the plants, the remainder being driven out into free space. This observation would suggest that blowing dust over the tops of the plants is a wasteful way to utilize the dust since only a little more than half the dust is attracted toward plant surfaces under the best circumstances. On the other hand, in the inner regions all of the dust is attracted toward some plant surface. The impressive visual effects of electrostatics when blown over the top would be diminished if the dust were blown entirely to the inner regions, but control capabilities may be considerably enhanced for some pests.

A reduction of air volume increases field intensities. In the laboratory it

POTENTIAL Vs DISTANCE FROM CENTER OF SPHERE

MAGNITUDE OF FIELD INTENSITY vs DISTANCE FROM CENTER OF SPHERE

FIG. 3(a) (Left) Upper curve shows the potential distribution along a radius of a hollow spherical cloud with inner boundary at zero potential and outer boundary floating. The lower curve shows the potential distribution of the same cloud with the outer boundary at zero potential. • FIG. 3(b) (Right) Field intensity distribution along a radius of the cloud of Fig. 3(a). A greater field intensity results from the cloud with the floating boundary.

has been found that a nozzle air velocity of 30 mph results in approximately double the deposit of a nozzle air velocity of 90 mph when dust is charged. This is a result of three factors that have not been completely analyzed as to their relative importance: (a) the erosion of dust (wind and sand blast effects) is less at low velocities than at high velocities, (b) the concentration of mass per unit volume of air is greater at low velocities than at high velocities (same quantity of dust dispersed in smaller volume of air at low nozzle velocities as compared to high velocities), and (c) the charging time in the nozzle is greater at low velocities than at high velocities. The longer charging time and the increased charged dust concentration results in approximately three times the charge density per unit volume of air at the lower nozzle air velocity. It is presently believed that the gain in deposit at low velocities is largely the result of the increased charge and mass density per unit volume of air.

In the field, the usual nozzle air velocity for dusting is from 90 to 120 mph in order to reduce crosswind effects and to obtain penetration of the foliage. If a means of reducing the influence of crosswinds and assuring adequate penetration at substantially lower velocities were developed, then it is likely that substantially greater ratio of charged to uncharged deposits than the present 2:1 ratio would be obtained.

The induced charge on a boundary determines the electric field intensity in the charged cloud just off the boundary surface. The general equation [2] for the field intensity of a spherical charged cloud, when evaluated at the interior cloud boundary where $r = a$, is $E = -V/a$. This intensity of the electric field is independent of the field of all charges except that due to the charge of the interior boundary at $r = a$. We have seen that if a conducting body inside a charged cloud is not connected to ground, no electrical field forces will exist to cause deposition.

With a floating inner boundary, the charge on the sphere is zero and the electric field intensity just off the sphere at $r = a$ is

$$E = \frac{-Q_s}{4\pi\epsilon a^2} = \frac{-V}{a} = 0.$$

If a boundary is connected to ground or other source of charge such as a battery or capacitor of lower potential than the cloud potential, a charge opposite in electrical sign to that of the cloud will be induced upon the boundary and an electric field will be developed that will drive a particle of the cloud to the boundary.

Large charges may be induced on the surfaces of plant parts by bringing a charged conductor close to the plant. If the charged conductor has the same sign of charge on it as the charged particles are carrying, the induced charge on the plant part will attract the particles. The few attempts that have been made to utilize the electric fields resulting from the use of charged bodies (shields) next to plants have been disappointing for two reasons. The leaves form an electrical cage so that the charges are largely induced on the outer leaves of the plant, and most of the charge is induced on the edges of the leaves resulting in heavier deposits on the edges than on the remainder of the leaf surface. In addition, there has been a problem of the discharging of conducting shields by touching plant parts since the shields have to be relatively close to the plants to be effective. Shields or hoods made of nonconducting materials pick up a charge from deposited dust from the cloud and tend to increase the fields at the leaf surfaces. Shields of non-conducting materials will not discharge as completely as conducting shields when grounded by plant parts but have some of the same disadvantages of caging and fringing as do conducting shields.

Sections from parallel infinite planes with a uniformly charged cloud sandwiched between.

Potential distribution

Field intensity, and direction of force.

FIGURE 4.

Nevertheless, local fields can be developed very readily with charged bodies and the use of shields could be useful in cases where the fringing and caging effects are not objectionable.

The level of the charge density controls the magnitude of the electric forces available for particle deposition. Since the electric field intensity is linearly related to the charge density ρ, the charge density level is the single most important factor in the maintenance of an adequate deposition field.

For practical purposes, the charge is distributed in space by means of charge carriers. Air ions are the main charge carriers in the intense electric fields within the charging nozzles. Dust or spray particles are the main charge carriers in the clouds that are blown into the plant regions because only a relatively few free air ions are carried out of the charging nozzle along with the pesticide particles. The electric fields near the plant surfaces are formed from the charge density $\rho = nq$ coulombs per meter[3] of space, where n is the number of particles per unit volume with charge q coulombs on them.

The importance of efficient charging of the particles on the force of deposition is evident from the fact that for any particular configuration, the field intensity E is proportional to the charge density $\rho = nq$, and the force on the individual particle of charge q is proportional to nq^2.

As pointed out by Splinter (13) a criterion for evaluating relative deposition from any given electric field configuration is the distance a particle can move toward a surface per unit of time. This criterion is most conveniently expressed by the terminal velocity V_t of a particle in a viscous medium as given by Stokes's Law. Neglecting corrections for Reynold's number, the terminal velocity, $V_t = F/6\pi r'\eta$, where F is the force on the particle, r' is the radius of the particle and η is the viscosity of the medium. Deposition then is directly related to the force F on the particle and is proportional to q^2 when the electric field of the cloud is the result of charged particles only. This is substantially the case with present electrostatic dusters. Although theoretically the most effective way to increase electric fields is to increase the level of charge on the individual particles, as previously pointed out air ions are also charge carriers and can be used to create very intense electric fields. The actual quantity of electricity on the charged particles, which is responsible for the 100 percent increase in deposition of dusts in the field, is equivalent to less than 5 microamperes per crop row. Another 100 percent increase in deposition efficiency could be expected if the equivalent charge carried by 5 microamperes

of air ions per row could be effectively incorporated into the electric field next to the leaves. This has been done by Hampe (8) using a corona discharge above the plants for increasing deposition on the exterior leaf surfaces. Unfortunately the exterior leaves are seldom the most important surfaces to be coated for pest control. A practical means of injecting these air ions into the inner regions of the plant has not as yet been found.

The electric resistivities of both the deposition surface and the deposit material influence the electrical field intensity at the deposition surface. The local field intensity next to a boundary will be reduced by the IR drop across a highly resistive surface such as a wax coating on a leaf or an existing coat of dust. Calculations show that serious problems should not arise from this cause if the surface resistivity of the plant part is less than approximately 10^{10} ohm-cm², or if dust volume resistivities are less than approximately 10^{11} ohm-cm.

Experience indicates that trouble is unlikely from plant surface resistivities under normal field operation. However, in the laboratory Hood and Sasser (9) found that dry peanut kernels had such a high skin resistance (90,000 megohms measured between ends of peanut) that dust could not be made to deposit on the peanut kernel when they were lying on a grounded belt beneath a charged needle point. In this situation the current density was great enough (on the order of $1\mu A/cm^2$) that the IR drop prevented normal deposition. The difficulty was overcome by giving the kernels a five-second exposure to low pressure steam. The peanut skin resistance was lowered by a factor of a hundred by this treatment and normal deposition of charged dust resulted. It is conceivable that some kinds of plants under drought stress could present a surface resistivity problem if air ions were used to increase the charge density.

The volume resistivities of most dusts and spray liquids are generally below 10^{11} ohm-cm; however, resistivities of this order and higher have been observed (12), and there is a possibility of difficulties from this source.

The electric fields are transients. All of the electric fields previously discussed considered the charge density to be uniform throughout the cloud at time zero. It is recognized that this simplifying assumption is approximated only under conditions of high turbulence, low charge levels, and the absence of significant inertial forces. The authors have not attempted to mathematically rationalize the disposition of the fields after an initially uniform

Charged cloud next to a single grounded disk.

Potential distribution

Field intensity, and direction of force.
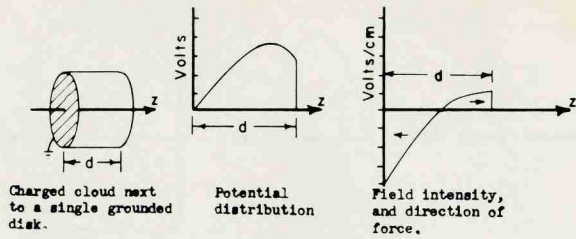
FIGURE 5.

cloud was placed between the boundaries at time $t = $ zero.

A qualitative analysis of the disposition of the field after time t equals zero would suggest that since the electric fields, particle forces, and particle terminal velocities are greatest near a grounded boundary, the particles move out of that part of the cloud near the boundary much faster than they move into the depleted region. After time Δt the charge density would be greater in the center of the cloud than near the boundaries. This would mean a lesser field intensity and forces at the boundaries than for a uniform charge density. The total charge level of the cloud would be reduced by the charge lost by deposition. It would appear that at the boundaries the calculation for a uniform charge density would represent the maximum field strength that would be expected after the start of deposition from a cloud of uniform charge density.

If charge densities are increased at the boundary surfaces by inertial or gravity forces the electric fields are correspondingly increased.

Summary

Electric field potentials and intensities have been calculated and verified experimentally for spherical configurations of clouds and boundaries with uniform charge densities. The electric fields of clouds with planar boundaries have been developed. The more im-

portant factors influencing the strength of the electric deposition fields have been described and an estimate of the magnitude of their influence made in the context of presently available equipment for crop protection.

An attempt has been made to appraise the limitations and the potential of the process as it is interpreted from a study of the electric fields of uniform charge density.

APPENDIX

Calculations of Electric Fields for a Spherical Cloud of Charge Particles.

Development of the General Potential Equation of a Conducting Sphere in a Charged Dust Cloud by Method of Superposition

The general equations [1] and [2] were developed stepwise by first calculating the potential throughout a positively charged spherical cloud and then superposing the potential distribution of a concentric spherical negatively charged cloud of smaller size. This provided a cavity within the larger positively charged cloud with no charge contained in the cavity. The third step was to suppress the outer boundary of the cloud to zero potential by adding a negative charge to the outer boundary. The fourth step was to insert in this hollow positive cloud a conducting sphere of the same radius as the cavity in the cloud and carrying the charge

Charged cloud sandwiched between two conducting disks.

Potential distribution

Field intensity, and direction of force.
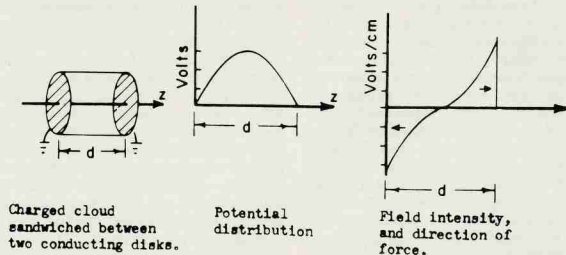
FIGURE 6.

necessary to raise or lower the potential to the desired value on the surface of the sphere. The final step was to add a charge to the outer boundary to bring it back to zero potential again.

There are five distinct charge distributions contributing to the potential distribution of uniform spherical cloud of charged particles containing a concentric conducting sphere when the outside boundary of the cloud is suppressed to zero potential. The potentials from these five sources will be briefly discussed individually, and then the combined equation will be developed.

Definitions of Symbols

a = radius of a conducting sphere and cloud of negatively charged particles, where $a < b$

b = radius of a cloud of positively charged particles

$C_a = 4\pi\epsilon a$, capacitance of a sphere of radius a in a medium of absolute dielectric constant ϵ

$C_r = 4\pi\epsilon r$, capacitance of a sphere and cloud at radius r and absolute dielectric constant ϵ

ϵ_1 = absolute dielectric constant of medium inside of cloud of charged particles, $a \leq r \leq b$

ϵ_2 = absolute dielectric constant of medium outside of cloud of charged particles, $r > b$

ρ = charge density of cloud of positively charged particles, $a \leq r \leq b$

$-Q_a$ = total charge in cloud of negative particles of radius a

Q_b = total charge in cloud of positive particles of radius b

$-Q_s$ = total induced charge on sphere of radius a

$r_{U max}$ = radius at which a maximum of the potential occurs

U = total potential of the system

U_i = potential inside of cloud

U_o = potential outside of cloud

U_a = potential due to negative cloud of radius a and charge density $-\rho$

U_b = potential due to positive cloud of radius b and charge density ρ

$U_{(a+b)}$ = potential of hollow cloud formed by superposing the potential of a negative cloud of radius a onto the potential of a positive cloud of radius b . . . . $a < b$

$U_{(a+b)} \big|_{r=b}$ = potential of hollow cloud of positively charged particles evaluated at $r = b$

U_v = potential in space due to the charge Q_s induced on the surface of a conducting sphere of radius a

V = fictitious potential arising from dividing the charge Q_s induced on a conducting sphere by the capacitance of the sphere

V' = actual surface potential of sphere resulting from all induced charges and cloud space charge.

Boundary Conditions and Other Assumptions

$\epsilon_1 = \epsilon_2 = \epsilon$ = absolute dielectric constant of free space

$\rho = 0$ . . . . $r > b$

$\epsilon_1 \dfrac{\partial U_i}{\partial r} = \epsilon_2 \dfrac{\partial U_o}{\partial r}$ . . . . $r = b$

Limit $C_r U_i = \dfrac{4\pi \epsilon r U_i}{r \to b} = Q_b = \dfrac{4\pi b^3 \rho}{3}$

Limit $U_o = 0$
$r \to \infty$

$\nabla^2 U_i = \dfrac{1}{r^2}\dfrac{d}{dr}\left\{ r^2 \dfrac{\partial U}{\partial r}\right\} = -\dfrac{\rho}{\epsilon}$
. . . . Poisson's equation

$\nabla^2 U_o = \dfrac{1}{r^2}\dfrac{d}{dr}\left\{ r^2 \dfrac{\partial U}{\partial r}\right\} = 0$
. . . . Laplace's equation

Development of Potential Equation

The first electric field of interest is that of a uniform charge distribution throughout an unsigned spherical cloud of radius b and charge density ρ. The equations are developed by an application of Poisson's equation within the cloud and Laplace's equation outside of the cloud using standard procedures.

Upon integrating the above equations and applying the boundary conditions and limits, the final equation for a uniformly charged cloud of particles of charge density ρ is as follows:

$U_b = \dfrac{\rho b^2}{2\epsilon} - \dfrac{\rho r^2}{6\epsilon}$
. . . . $0 \leq r \leq b$ [12]

$U_b = \dfrac{\rho b^3}{3\epsilon r}$ . . . . . . $r \geq b$ [12a]

The second charge distribution is that of a smaller uniform cloud of radius a and charge density $-\rho$. The same boundary conditions hold for the small cloud of radius a as for the larger cloud of radius b, except that a is substituted for b for the smaller cloud.

The equations for the potential of the uniformly charged cloud of charge density $-\rho$ and radius a are as follows:

$U_a = \dfrac{-\rho a^2}{2\epsilon} + \dfrac{\rho r^2}{6\epsilon}$
. . . . $0 \leq r \leq a$ [13]

$U_a = \dfrac{-\rho a^3}{3\epsilon r}$ . . . . . . $r \geq a$ [13a]

The sum of the two clouds is given by the following equation where $a < b$:

$U_{(a+b)} = \dfrac{\rho}{2\epsilon}\left\{ b^2 - \dfrac{r^2}{3}\right\} - \dfrac{\rho a^3}{3\epsilon r}$
. . . . $a \leq r \leq b$ [14]

The third distribution of charge is due to the suppression of the potential to

zero at the outer cloud boundary by electrical grounding. This is brought about by placing a negative charge on the outer boundary such that its potential will just cancel the potential of the hollow cloud $U_{(a+b)}$ at the outer boundary with $r = b$. The value of potential

and limit $\dfrac{4\pi \epsilon r U_i}{r \to a} = -\dfrac{4\pi a^3 \rho}{3} = -Q_a$

tential that must be subtracted is $U_{(a+b)} \big|_{r=b}$. The equation developed for a hollow cloud with its outer boundary suppressed to zero is as follows:

$U_{(a+b)} - U_{(a+b)} \big|_{r=b} = \dfrac{\rho}{6\epsilon}(b^2 - r^2) + \dfrac{\rho a^3}{3\epsilon}\left\{ \dfrac{1}{b} - \dfrac{1}{r}\right\}$ . . $a \leq r \leq b$ [15]

The fourth potential distribution results from the surface charge on the sphere required to maintain a given arbitrary potential on the sphere. The introduction of the sphere into the cloud does not disturb the potential distribution within the cloud, or external to it, as long as there is no charge on the sphere. This is a direct consequence of the fact that the electrical potential of a point in space is defined by the work required to bring a unit positive charge from infinity or any place of zero potential up to the point. Thus, if there is no charge on the sphere when the sphere is inserted into the cavity of the cloud, there is no change in the work required to bring a charge to the sphere surface or the potential represented by the work. When a charge is placed on the sphere it does modify the work and the potential. If the charge is positive, the work required to bring a unit positive charge from a place of zero potential to the sphere is increased and thus the potential is greater. The opposite is true when the charge on the sphere is negative.

For purposes of deposition, the potential of the deposition surface (in this case, the sphere) will need to be less in magnitude than the potential of the surrounding cloud. Thus, for a positively charged cloud, a negative charge would have to be placed on the sphere. The magnitude of this charge is given by

$-Q_s = -VC_a = -V4\pi\epsilon a$ . . [16]

where $-V$ is the potential that will be on the sphere due to the charge on the sphere in the absence of any neighboring charges. The charge is negative and thus the potential U_v due only to the charge on the sphere is:

$U_v = \dfrac{-VC_a}{C_r} = \dfrac{-V4\pi\epsilon a}{4\pi\epsilon r} = \dfrac{-Va}{r}$
. . . . $r \geq a$ [17]

$U_v = -V$ . . . . . . $r \leq a$ [17a]

The addition of the term describing the potential due to the charge on the sphere causes the boundary value at $r = b$ to be depressed to less than zero. This may be compensated for by adding a positive charge to the outer boundary of a value $V4\pi\epsilon a$.

The charge added at the boundary will have a potential of

$$U_v = \frac{VC_a}{C_b} = \frac{V4\pi\epsilon a}{4\pi\epsilon b} = \frac{Va}{b}$$

at the outer boundary. $r = b$ [17b]

The completed equation for a uniform spherical cloud of positively charged particles enclosing a concentric conducting sphere, when the cloud boundary is suppressed to zero potential is as follows:

$$U = U_{(a+b)} - U_{(a+b)}\big|_{r=b} - \frac{Va}{\rho} + \frac{Va}{b} \dots \dots \dots a \leqslant r \leqslant b$$

$$U = \frac{\rho}{6\epsilon}(b^2 - r^2) + \frac{\rho a^3}{3\epsilon}\left\{\frac{1}{b} - \frac{1}{r}\right\} - \frac{Va}{r} + \frac{Va}{b} \dots a \leqslant r \leqslant b \ [1]$$

This equation may be evaluated for V for any arbitrary value of V', the potential of the surface of this sphere, by solving the equation with $V' = U$ at $r = a$.

The field intensity $E = \dfrac{\partial U}{\partial r} = \dfrac{\rho r}{3\epsilon} - \dfrac{\rho a^3}{3\epsilon r^2} - \dfrac{Va}{r^2} \dots a \leqslant r \leqslant b \ [2]$

Calculations of Electric Fields for a Cloud of Charged Particles Between Infinite Planes

The field of a uniform cloud sandwiched between two parallel infinite conducting planes at zero potential was developed by Splinter (13). Plots of the potential and the field intensity versus distance from the plan are shown in Fig. 4. From Poisson's equation in rectangular coordinates

$$\nabla^2 U = \frac{\partial^2 U}{\partial x^2} + \frac{\partial^2 U}{\partial y^2} + \frac{\partial^2 U}{\partial z^2} = -\frac{\rho}{\epsilon}$$

The field is independent of x and y coordinates because the space between the planes is completely shielded from external electrical fields. $\nabla^2 U + \dfrac{\rho}{\epsilon} = 0$ is an ordinary differential equation of second order independent of x and y, thus $\dfrac{\partial^2 U}{\partial z^2} = -\dfrac{\rho}{\epsilon}$

If ρ is assumed constant, the following boundary conditions must be satisfied:

At $z = 0$, $U = 0$

$z = d$, $U = 0$, where d is the distance between plates

$z = \dfrac{d}{2}$, $\dfrac{\partial U}{\partial z} = 0$

Integration with respect to z gives

$\dfrac{\partial U}{\partial z} = \dfrac{-\rho}{\epsilon}z + C_1$, where C_1 is an arbitrary constant of integration

But $\dfrac{\partial U}{\partial z} = 0$ at $z = \dfrac{d}{2}$; therefore

$\dfrac{-\rho}{\epsilon}\dfrac{d}{2} + C_1 = 0$, or $C_1 = \dfrac{\rho d}{2\epsilon}$

Then $\dfrac{\partial U}{\partial z} = -\dfrac{\rho z}{\epsilon} + \dfrac{\rho d}{2\epsilon}$

Integrating again with respect to z yields

$U = -\dfrac{\rho z^2}{2\epsilon} + \dfrac{\rho dz}{2\epsilon} + C_2$, where

C_2 is a constant of integration.

But $U = 0$ at $z = 0$; therefore
$C_2 = 0$.

Therefore $U = -\dfrac{\rho z^2}{2\epsilon} + \dfrac{\rho dz}{2\epsilon} =$

$\dfrac{\rho}{2\epsilon}(dz - z^2) \dots \dots \dots$ [18]

gives the potential at any point between the planes.

The electrical field intensity is

$$E = -\frac{\partial U}{\partial z} = \frac{\rho z}{\epsilon} - \frac{\rho d}{2\epsilon}. \quad [19]$$

References

1 Atwood, Stephen S. Electric and magnetic fields. 3rd edition. John Wiley & Sons, New York, N.Y., p. 475, 1949.

2 Bowen, Henry D., Hebblethwaite, Peter, and Carleton, W. M. Application of electrostatic charging to the deposition of insecticides and fungicides on plant surfaces. Agricultural Engineering 33:347-350, June 1952.

3 Bowen, Henry D. Electric and inertial forces in pesticide application. Unpublished Ph.D. thesis, Michigan State University, East Lansing, 130 number leaves, 1953.

4 Bowen, H. D. and Splinter, W. E. Electrostatically charged sprays and dusts. Official proceedings 1963 Beltwide Cotton Production Conference, Dallas, Sponsored by National Cotton Council, January 1963.

5 Brazee, R. D. Some basic measurements for analysis of electrostatic dust precipitation. Unpublished Ph.D. thesis, Michigan State University, 81 numbered leaves, 1957.

6 Brooks, F. A. The drifting of poisonous dusts applied by airplanes and land rigs. Agricultural Engineering 28:233-239, June 1947.

7 Casselman, T. W., Thayer, P. L., and Geming, W. G. Dusting pole beans. Florida Grower and Rancher, pp. 13 and 16, March 1963.

8 Hampe, Pierre. Le poudrage electrostatique des vegetaux. Reprint of the Proceedings of a conference of La Lique de Defense Contre les ennemis des Cultures. (translated by Peter Hebblethwaite) Paris, 19 pp., 1947.

9 Hood, C. and Sasser, P. E. Report on electrostatic dusting of peanuts. A special report prepared for James Keel, Keel Peanut Co., Greenville, N.C., on a method for dusting seed peanuts using electrostatics, 8 pp, 1959.

10 Jeans, Sir James Hopwood. The mathematical theory of electricity and magnetism, 5th edition. The University Press, Cambridge, 645 p, 1933.

11 Kellogg, Oliver Dimon. Foundations of potential theory. Frederick Ungar Publishing Co., New York distributors.

12 Penney, G. W. Electrostatic precipitation of high resistivity dust. Transactions of the American Institute of Electrical Engineers, 70: 1192-1196, 1951.

13 Splinter, W. E. Deposition of aerial suspensions of pesticides. Unpublished Ph.D. thesis, Michigan State University, East Lansing, 164 numbered leaves, 1955.

A - Plant Diameter
B - Head Diameter
C - Length of Leaf Stem
D - Plant Stem Diameter

VERTICAL FORCE

PHYSICAL PROPERTY MEASUREMENTS OF CABBAGE

In addition to those on the drawing:
a) Head Weight

b) Force to cut stem
   (In region of leaf attachment)

c) Resistance to drop

d) Weight and diameter relationship

e) Head size distribution

f) Ratio of plant and trim weight to
   head weight

Figure 1
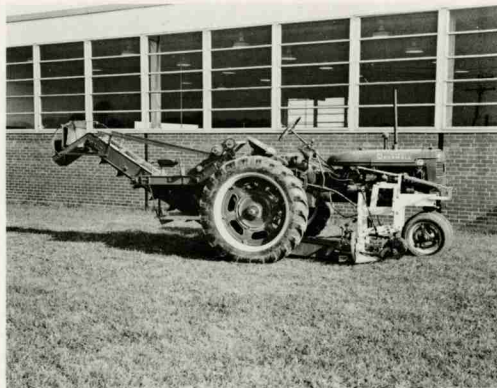
Figure 2. Overall view of experimental cabbage harvester.
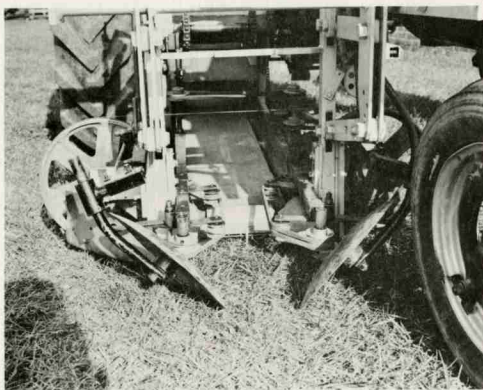
Figure 3. View of cutting mechanism from the front showing disks and head supporting device.
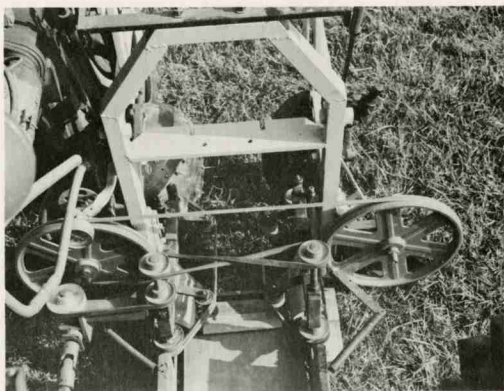
Figure 4. View of cutting mechanism from rear (operator's view) showing pulley arrangement for bandsaw blade and drive for head supporting device.
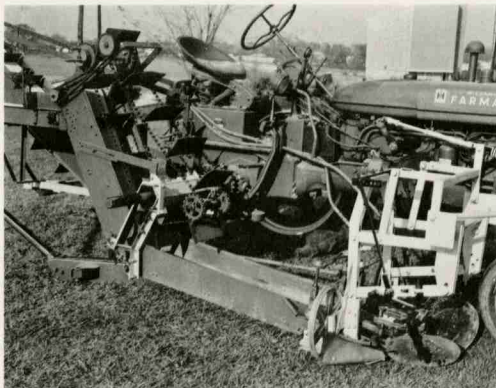
Figure 5. Arrangement of conveyors and elevating system about the rear axle.
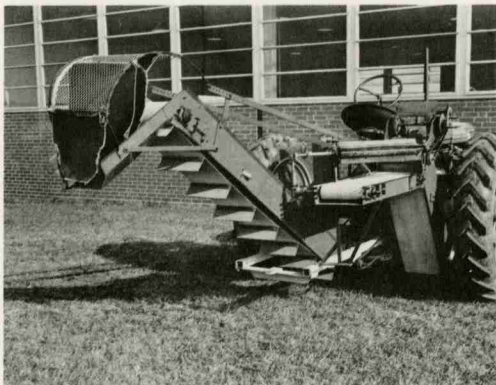
Figure 6. Right rear view of harvester showing loose leaf separator unit and trailer loading conveyor.
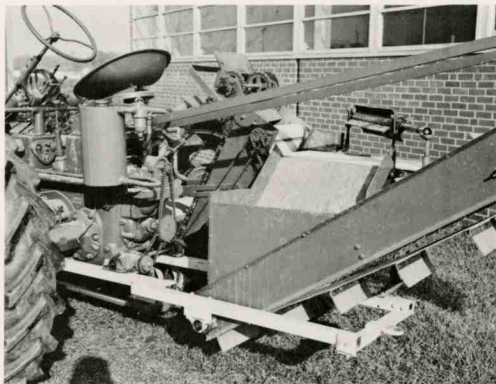
Figure 7. Left rear view of harvester showing hydraulic bandsaw
drive components and conveyor drive arrangement.

Figure 8. View of 1963 model experimental cabbage harvester
operating in the field.

FIGURE 2. TESTING MACHINE SET UP FOR COMPRESSION PLUNGER TEST
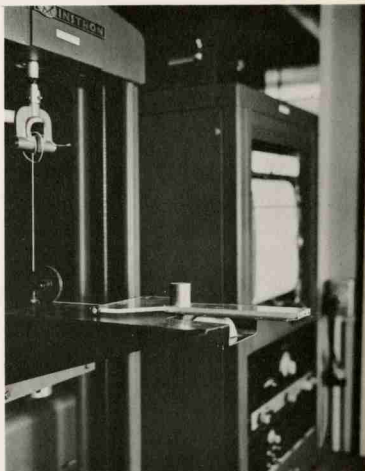
FIGURE 3. FRICTION COEFFICIENT MEASURING APPARATUS
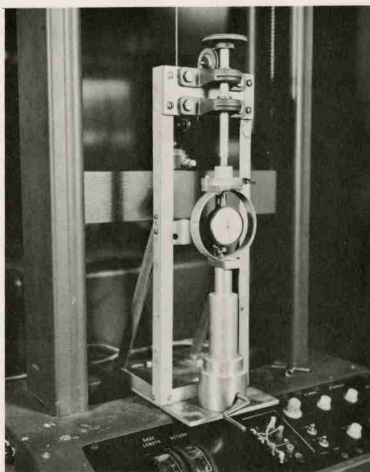
FIGURE 4. SKINNING APPARATUS
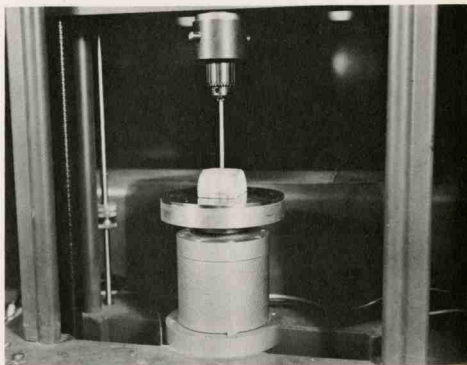
FIGURE 5. COMPRESSION PLUNGER TEST

THE CHARGING OF LIQUID SPRAY BY ELECTROSTATIC INDUCTION

By

S. Edward Law
Research Assistant
Department of Agricultural Engineering
North Carolina State University
Raleigh, North Carolina

and

Henry D. Bowen
Professor
Department of Agricultural Engineering
North Carolina State University
Raleigh, North Carolina

For Presentation at the 1965 Annual Meeting
AMERICAN SOCIETY OF AGRICULTURAL ENGINEERS

University of Georgia
June 20 - 23

THE CHARGING OF LIQUID SPRAY BY ELECTROSTATIC INDUCTION

Introduction

The application of agricultural chemicals in the form of sprays has distinct advantages as compared with application in the form of airborne dusts. For instance, metering is more easily accomplished with liquids, and many control chemicals are normally liquid.

The earlier sprays were applied using high amounts of diluent per acre with most of the spray droplets having greater than 400 microns diameter. The introduction of more finely atomized concentrated sprays having droplet diameters less than 300 microns brought both advantages and disadvantages effected by the significance of the decreasing droplet size.

Various investigators have shown that the chemical effectiveness of deposited pesticide sprays increases as droplet size decreases. However, the probability of a droplet depositing on a target surface decreases with droplet size. Furthermore, the harmful problem of spray drifting increases dramatically with decreasing droplet size.

Hence, in order to improve the overall plant coverage by concentrated sprays and especially to increase the deposition of the more effective smaller diameter droplets of the spray spectrum, the electrification of spray droplets and their consequential electrostatic precipitation was attempted.

Two physical phenomena, ionized field charging and electrostatic inductive charging appeared to offer much practical adaptation to the electrification of sprays. Although ionized field particle charging had already been well developed, little work appeared to have been done in applying electrostatic induction to the charging of particles. It was

further realized as an advantage that ideal charging by electrostatic
induction required no current from a high voltage power supply; whereas,
ionized field charging necessitated currents on the order of 100 micro-
amperes at voltages generally greater than 10 kilovolts. Thus, the study
was limited mainly to charging by induction.

Significance of Spray Droplet Size

The choice of droplet size for field spraying is at best a compromise.
On the one hand small droplets of pesticides less than 30 microns diameter
have been shown to exhibit higher chemical effectiveness than larger drop-
lets when deposited; while on the other hand, deposition of these small
droplets under field conditions is extremely poor.

The work of Ennis and Williamson (7), Figure 1, is representative of
the research on droplet size versus effectiveness. Although the smallest
droplets that Ennis and Williamson studied were approximately 50 microns,
the trend of increasing effectiveness with decreasing droplet size still
persisted at that diameter.

Further it has been shown that in applications where control is pro-
portional to the surface area of the pesticide that for equal protection
any reduction in particle radius allowed an equal percent reduction in the
weight of the pesticide deposited (13).

While small droplet size is desired for the preceding reasons, it has
the disadvantage of a reduced linear momentum which affects a droplet's
ability to impinge upon a surface. All sprays entrain a mass of air which
moves along with the droplets. In order for a droplet to reach the target
surface, it must have sufficient momentum to penetrate the accompanying air
stream which flows around the surface. If a droplet nears the target
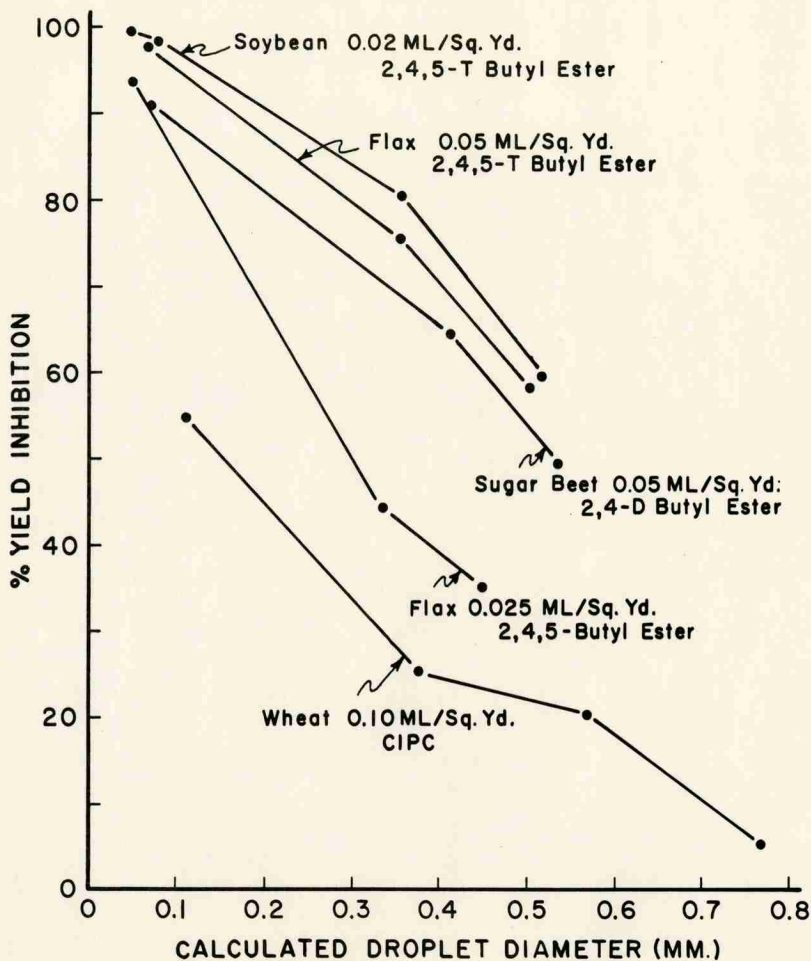
Figure # 1.

Yield of 4 crops as influenced by different droplet-size treatments with selected herbicides. (W. B. Ennis, Jr. & Ralph E. Williamson)

surface with insufficient momentum, the centripetal acceleration imparted to it due to the viscosity of the deflecting air stream changes its direction of velocity enough to cause it to travel parallel to the surface and depart with the air stream. Since linear momentum varies directly with mass and velocity, the smaller droplets of a spray spectrum may not impinge unless they have high velocity. Figure 2 illustrates this dependence of impingement upon droplet momentum for two values of approach velocity toward a 1/8 inch diameter stem (3). Percent catch refers to that fraction of an approaching air stream having the same cross-sectional area as the stem which is cleared of droplets of a particular diameter. Percent catch is seen to decrease with drop diameter; the rate of decrease becomes greater as diameter falls below about 40 microns.

Methods of Producing Electrified Sprays

A search through physics journals reveals voluminous works listed under "spray electrification." However, this nomenclature is generally reserved for a clearly defined mechanism by which water and certain other liquids become electrified whenever their surfaces are disrupted such as by spraying or bubbling. This research in spray electrification was of little value in the present study because the droplets investigated were generally less than one micron diameter and their charge-to-mass ratios were only about 6×10^{-10} coulomb per gram of water atomized.

Chapman (4) investigated the charging by dispersion phenomenon with spray droplets produced by an ordinary brass atomizer using techniques employed in the Millikan oil drop experiment. Drops ranged in diameter from 3 microns to 10 microns with average absolute electronic charge of 125 to 600 respectively for pure water. Charge was found to vary roughly
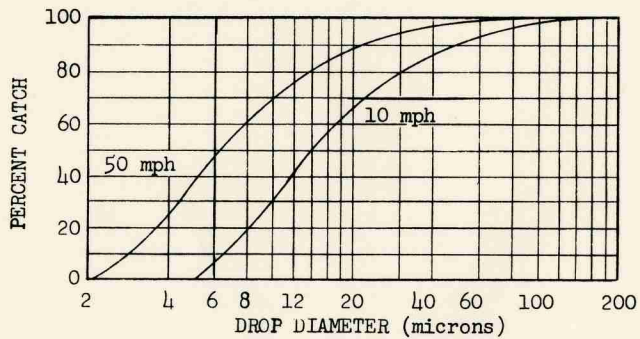
Figure 2 Dynamic catch versus droplet size
for 1/8 inch diameter stem
(Brooks, 1947, p. 235)

in a linear manner with diameter. In addition, for drops of the same size a rough parallelism was noted between droplet charge and dielectric constant of the various liquids used. No preference for either sign of charge was evident; an equal number of droplets of a given size were charged positively as were charged negatively. This is referred to as symmetrical charging.

Vonnegut and Neubauer (15) produced streams of highly charged liquid droplets of 100 microns diameter by electrical atomization. When they applied potentials of 5 kilovolts and greater to water in small capillary tubes, normal formation of droplets of about a millimeter diameter and at a rate of a few a minute was changed into formation of 100 micron droplets at a rate of about 100 per second. This change was attributed to the fact that during droplet formation electrical charges on a droplet's surface repel each other and cause a force opposing surface tension. It was further observed that highly charged aerosols having a particle diameter of 2 microns or less could be produced if positive potentials were applied to capillaries containing liquids having low electrical conductivity.

Blanchard (2) investigated the charge on sea water sprays produced from bubbles which moved upward and burst at an air-sea water interface. By applying an electrical potential to a brass field piece held above and parallel to the free surface of the grounded liquid, the droplets became charged by induction as they separated from a bubble in the presence of an electric field of 50 to 300 volts per centimeter. The results are presented in Figure 3. A charge of 10^6 electrons was achieved on 100 micron droplets. For a given size droplet, the induced charge was found to be constant for field intensities of 50 to 300 volts per centimeter. With the highly conductive sea water, this indicated that the charge separation was limited by
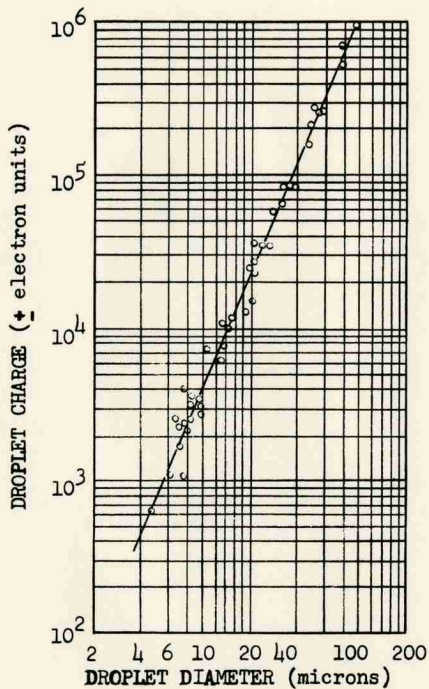
Figure 3 **Induced droplet charge versus diameter for
sea water droplets produced from the burst-
ing of bubbles in the presence of an
electric field** (Blanchard, 1955, p. 335)

some back discharge or current flow mechanism, and not determined entirely by polarization in the electric field.

In studying the effect of electric charge on raindrop formation by the coalescence of smaller water drops, Telford et al. (14) produced sprays of 130 micron diameter droplets by shearing water tangentially from the edge of a rapidly rotating smooth circular disk. A charging wire positioned just beyond and above the disk's periphery provided an electrostatic field for inducing charge onto the droplets. Charges as high as 3×10^{-13} coulombs or 1.88×10^6 electronic charges were imparted to the droplets by induction.

Applications of Electrified Sprays

The use of charged sprays to enhance deposition through the action of electrostatic precipitation has found widespread acceptance in industry. Ransburg first introduced the technique for paint spraying in 1940. The paint was originally sprayed with conventional spray guns into an ionized field set up between an electrode system of fine corona discharge wires and the grounded object being coated. The individual droplets were charged to the sign of the discharge electrodes and traveled along the electrical lines of force to the object being coated. More recent models use a specially designed spray gun incorporating a single finely pointed discharge wire of less than one inch length protruding from the nozzle end of the gun. In a third model paint is fed to the center of a rapidly rotating high potential disk or bell-shaped atomizer and is flung tangentially from the edges.

Savings as high as 70 percent in coating materials are claimed to result from use of the above processes. However, direct current power supplies having potentials in excess of 90 kilovolts and output currents up to 10 milliamperes are required. This is generally accomplished in a

completely oil immersed system wherein 220 volts, single phase, 60 cycle input is transformed to 120 kilovolts and then given half-wave vacuum tube rectification. The high cost and immobility of such industrial equipment renders it impractical for agricultural applications.

Wampler and Hoskins (16) in trying to elucidate the role of electric charges produced during spraying of pesticides, attempted the electrostatic precipitation of charged aqueous sprays of lead arsenate. Various degrees of droplet charging were possible by applying potentials between $\pm$ 150 volts d.c. to the metal spray nozzle, and the effect upon subsequent deposit onto a waxed 4 inch copper square was analyzed. They found no deposition increase due to charging the spray droplets. However, calculations based on their data indicated charging of only about 3.61×10^{-9} coulombs per gram of liquid sprayed. This was a very small charge and could not be expected to measurably increase deposit. It was only about 4 times greater than the charge per gram attributed solely to the surface disruption of the spray electrification phenomenon.

Theory of Inductive Spray Charging

Consider a grounded metal nozzle spraying a conducting liquid. For many commercial nozzles, especially those in which the liquid is hydraulically atomized, the liquid emerges from the orifice in a continuous sheet and breaks up into small droplets at some short distance from the orifice. The disruption of the sheet results from surface friction between the sheet and the surrounding air and from surface tension being overcome as the sheet diverges. This condition is shown exaggerated in Figure 4.

Suppose as in Figure 4 that a body B possessing a given amount of net positive charge is brought into the vicinity of the orifice without touching
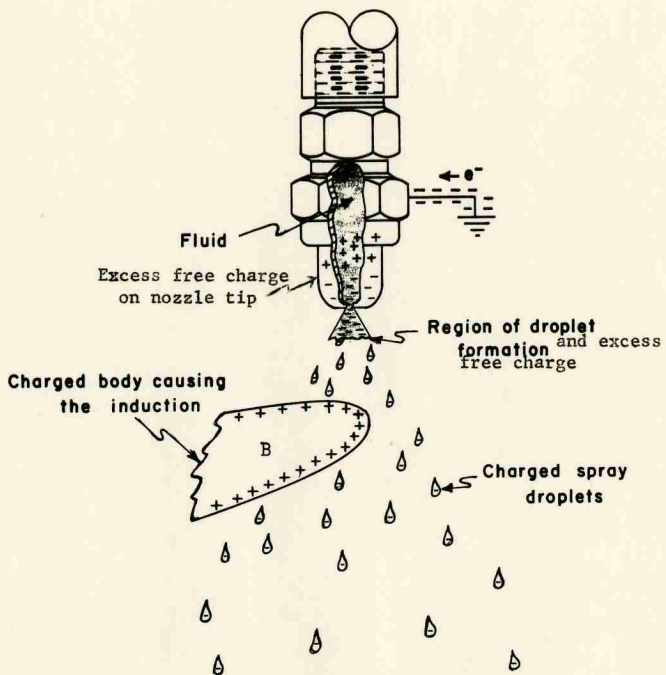
Figure 4   Induction charging of spray showing
charge distribution for a conducting
nozzle-spray system

the continuous liquid sheet. The resulting electrostatic forces of attraction will cause free electrons to flow from ground through the nozzle and liquid to the end of the continuous sheet and produce a region of excess negative charge there. This excess charge is necessary to maintain the nozzle and liquid at ground potential in the presence of the positively charged body B. Since the droplet formation region possesses an excess negative charge, droplets forming there are negatively charged. As these droplets carry free electrons from the nozzle-spray system, the same quantity of electrons enters the system from ground.

At electric field intensities less than those required for cumulative ionization of air, body B will retain its original charge if the negatively charged spray droplets all pass by it without contact. However, if some droplets do contact body B, part of the original charge on B will be neutralized. For practical applications this would necessitate a power supply to provide a neutralization current to body B in order for it to maintain its original amount of charge.

In order to maximize the net charge induced onto the spray, it is necessary to place the largest amount of opposite charge as near as possible to the droplet formation region. For a given spray liquid, this charge situation will maximize the force tending to transfer an electrical charge onto a liquid droplet at the instant of droplet formation. Coulomb's inverse square law describes this force when integrated over all charge distributions concerned.

If the inducing charge Q resides on a conducting electrode of capacitance C which is held at potential V, the capacitance relation indicates that in order to maximize Q at a given potential, the capacitance should be

maximized. However, capacitance is directly related to conductor area; hence, the area of the conductor on which the inducing charge resides should be maximized.

For an electrically conducting nozzle the excess free charge induced onto the orifice end of the nozzle tends to "cover" a portion of the inducing charge Q. Electrical lines of force from the inducing charge distribution which terminate on the nozzle's free charge are, thus, ineffective for transferring charge to the droplet formation region of the liquid. Since a dielectric material contains no conduction electrons, electrical lines of force from the inducing charge could terminate only on the bound surface charge due to polarization of a dielectric nozzle. Thus, theoretically, a dielectric nozzle would be desirable for inductive charging of sprays.

The cross section produced by a plane intersecting a hollow cone spray pattern near the droplet formation region and perpendicular to the axis of the spray cone, reveals two liquid-free regions of space into which inducing bodies could be placed. An electrostatic field could be established between the droplet formation region and inducing electrodes of the following types placed concentic with the spray axis:

(a) A conducting sphere placed within the hollow cone region.

(b) A conducting toroid positioned just off the outer circumference of the spray pattern.

(c) A combination of the cone and toroid.

For any given potential on an induction electrode, the electric field intensity at points within the electrostatic field between the induction electrode and grounded conductors of the nozzle-spray system will increase with decreasing electrode separation. At a minimum separation, dependent

upon potential, for fields of uniform intensities, the dielectric strength of the field medium will be exceeded, and a self-sustaining gas discharge will be initiated by a spark. In the case of fields of non-uniform intensities, corona discharge may precede electrical breakdown of the entire field gap. Such discharges reduce the effectiveness of the electro-static inducing field. It is known that increasing the water vapor content of air increases the voltage gradient necessary for dielectric breakdown (1, 8, 10). Thus, the often used breakdown value of 30 kv./cm. for dry air is also safe to use for the liquid spray laden air in determining critical induction electrode separation distances. Breakdown will, how-ever, occur prematurely if the induction electrode becomes wet since the surface gradient necessary for spark-breakdown is greatly lowered for water-sprayed conductors (11).

Corona discharge may result when dielectric breakdown of some local portion of a nonuniform electrostatic field occurs at a potential difference less than that required for a spark to bridge the entire gap. The limited region of failure will be just off portions of electrodes which have very small radii of curvature since strong local fields occur there. The self-sustained visible discharge occurring in the region of failure is known as corona. When corona is present, a major portion of the field conducts a unipolar current. Particles traveling through such unipolar current regions become highly charged to the sign of the discharge electrode by ionic attachment. Corona discharges may become established at sharp metal points on the induction electrodes. This is not difficult to overcome by dielectric encapsulation. Further, it is known that corona from a high potential water drop can occur (6, 17). A water drop on a wet induction electrode is drawn

to a sharp discharge peak under the influence of the high electric field in which it finds itself. This cannot be overcome by dielectric encapsulation of the electrode as before. Further, water sprayed onto a metal electrode lowers the voltage at which corona initiates (11). Thus, the surface of an induction electrode must be kept water-free if a high-value electrostatic induction field is to be maintained.

The detrimental result of corona will now be briefly discussed. Electrostatic induction always charges a particle to the sign opposite that of the inducing charge. Ionized field particle charging imparts the same sign charge to the particle as the polarity of the corona discharge electrode. Thus, if corona becomes established at an induction electrode, the spray will be acted upon by two opposing charging mechanisms. A particular potential, characteristic of each electrode configuration, exists at which the two charging mechanisms exactly nullify each other. At this null potential the spray will receive no net charge. At higher potentials than this, ionized field charging will dominate; that is, a polarity reversal of the sign of the net spray charge will occur.

Experimental Analysis

Various induction electrodes were tested in conjunction with two commercial hollow cone spray nozzles. One nozzle (Spraying Systems ¼ TTX3) was constructed of brass and the other (Spraying Systems ¼ NK3) was constructed entirely of a nonconductive plastic material having the trade name Kralastic. The manufacturer claimed similar atomizing and discharge performance for the two nozzles. Flow rate at 80 p.s.i. was given as 4.1 gallons per hour and median number droplet diameter as approximately 51 microns.

Variable potentials were applied to the induction electrodes by a 125 kilovolt, full-wave rectified, d.c. power supply. The charged spray was

directed into an electrically insulated metal box where it discharged through a microammeter to ground. This spray discharge current was the criterion by which the degree of spray charging was determined.

In order to test the hypothesized superiority of the dielectric nozzle, the following experiment was conducted. A 5/16 inch diameter spherical induction electrode was installed on a bent glass holder and set at a 9 mm. gap from the nozzle orifice on the spray axis. Four replications of spray discharge current were made at each increment of positive voltage for both the metal and the dielectric nozzle. Results appear in Figure 5. The means of the current for the dielectric nozzle were found to be significantly greater in magnitude at the 1% level of student's t for voltages of 1.5 to 7.0 kilovolts.

Two models of an induction electrode were constructed and tested in which a metal sphere and a toroid were positioned at fixed distances relative to each other and connected by a metal rod. Hence, both the sphere and toroid were held at the same high potential. The rod was bent so that it intercepted only a small percent of the droplets at a point where the spray cone had diverged. The common geometric design of the electrodes differed only in dimensions. The larger model A electrode was secured to a plexiglas insulating tube and mounted on a field sprayer for field testing as shown in Figure 6. The one ionized field charging head used as a comparison consisted of a high negative potential discharge electrode replacing the sphere and insulated from the toroid which was grounded.

In the laboratory positive potentials up to spark breakdown were applied to the induction electrodes A and B and negative potentials were applied to the ionized field discharge electrode, and spray discharge currents were measured. Results appear in Figure 7.
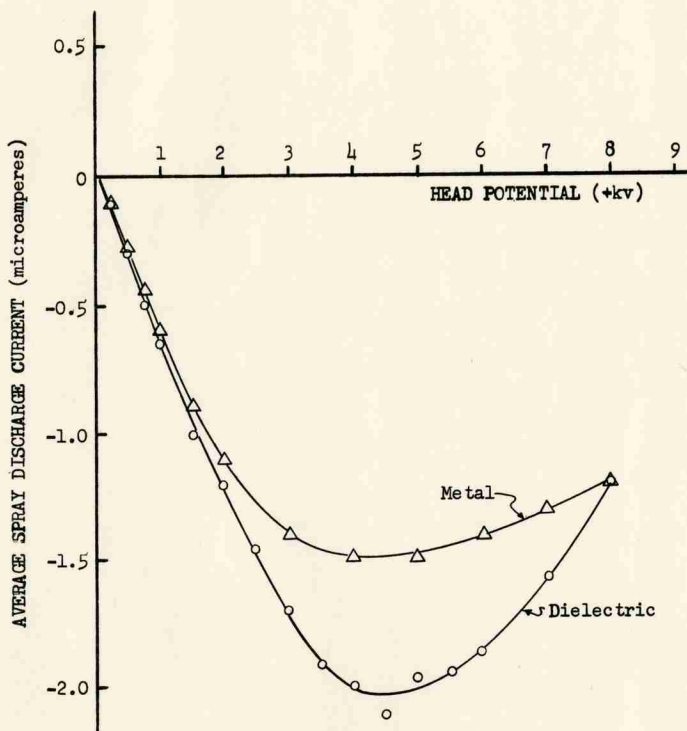
Figure 5 Average spray discharge currents for metal
and dielectric nozzles

1" Spray boom pipe

1⅜" galv. thin wall tubing
with washer soldered on
top

³⁄₁₆"

³⁄₈"

Teejet ¼TTX-3
Hollow cone spray
nozzle

1" dia. steel
sphere

⁷⁄₃₂" dia. steel ring,
O.D. 1¹¹⁄₁₆"; I.D. 1¼"

⅛ dia. brass rod

CROSS SECTION OF ASSEMBLY

Hose clamp

⅛"x 2"x 2" Plexiglas
tubing

High voltage
cable connection

SIDE VIEW
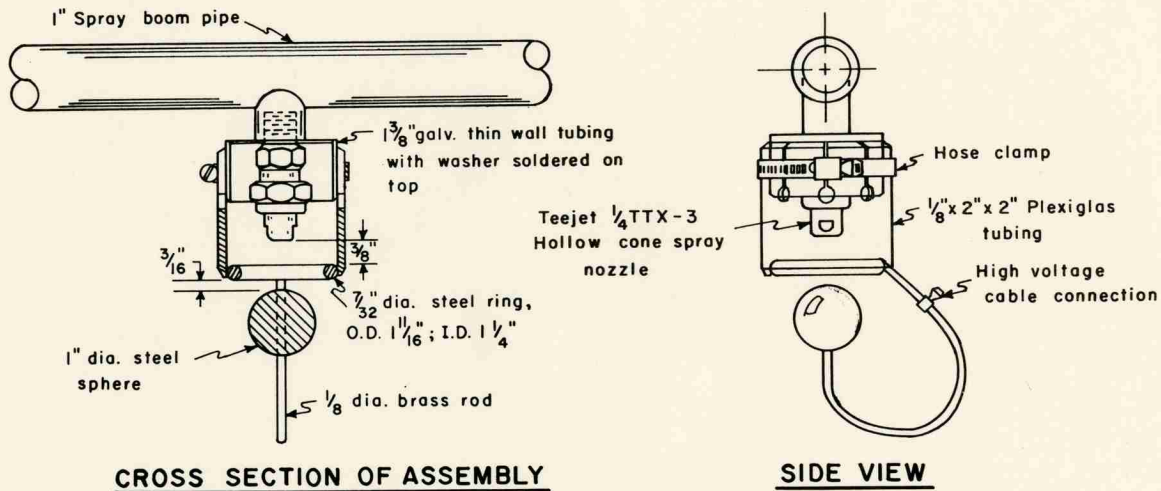
Figure 6   Induction head for field testing of plant coverage by charged sprays
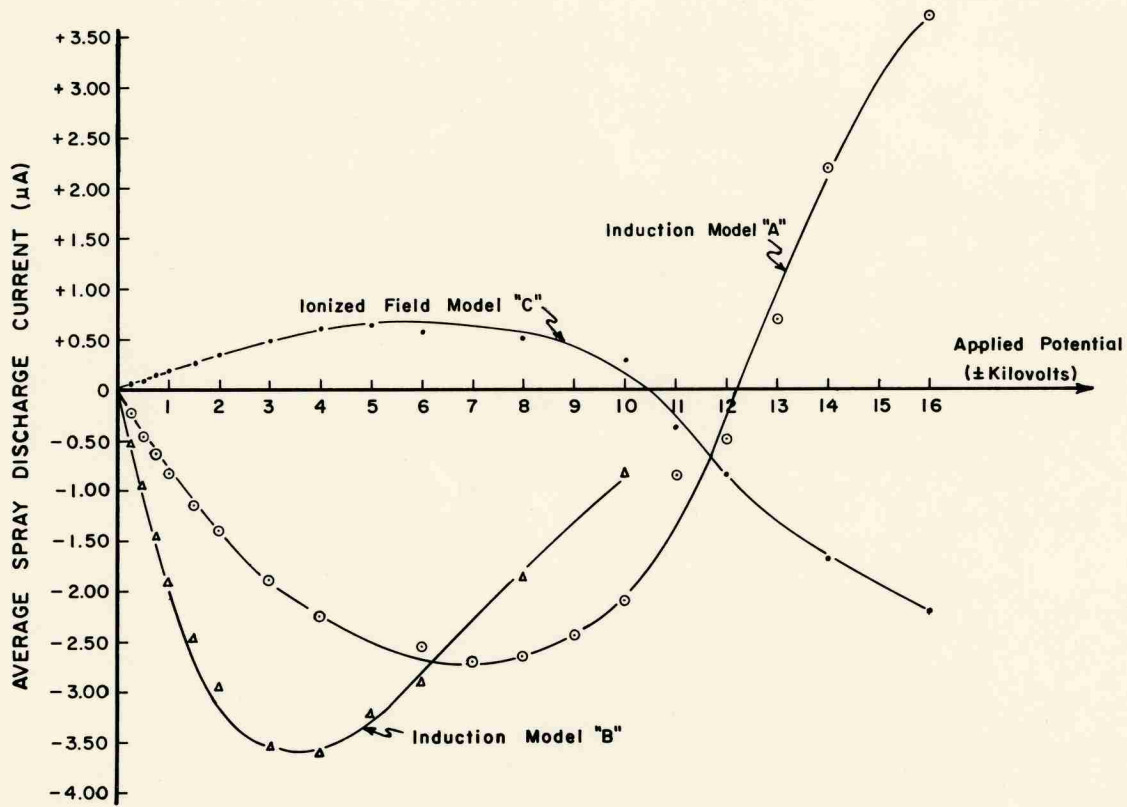
Figure 7 Average spray discharge current versus head potential for induction heads model A and B and for the ionized field head

For the model A induction head, the spray had a negative charge induced upon it at lower head potentials by the positive potential head. A maximum average spray discharge current of -2.70 microamperes occurred at +7 kv. The spray discharge current then decreased rapidly in net negative charge and actually equaled zero net charge at about +12.2 kv. At voltages above +12.2 kv the spray carried a net positive charge; hence, a polarity reversal of the spray current occurred.

For the model B induction head the spray also had a negative charge induced upon it at lower head potentials by the positive potential head. A maximum average spray discharge current of -3.60 microamperes occurred at +4 kv. Spray discharge current decreased rapidly with increasing voltages above +4 kv. Spark-breakdown occurred before a spray current polarity reversal could occur.

The negative ionized field discharge electrode appeared to have induced net charge of the opposite sign to it onto the spray at voltages less in magnitude than -10.5 kv. Corona discharge onset appeared to have been at approximately -3 kv since at this potential the first measurable current to the discharge electrode was noted; and, also, at -3 kv the curve in Figure 7 became non-linear. The two charging phenomena exactly nullified each other at approximately -10.5 kv resulting in a zero spray discharge current. Ionized field charging dominated at potentials above the spray current polarity reversal potential at -10.5 kv giving spray current of the same sign as the discharge electrode.

Experimentally Observed Corona

The existence of corona discharges at the high voltage induction electrodes was experimentally witnessed and established as a limiting

factor of the degree of inductive spray charging. Ionized field spray charging by corona currents from induction heads is indicated by the change in the sign of the slopes of induction electrode curves of Figure 7. Many more curves of spray current versus induction electrode potential for spherical electrodes at various nozzle-separation distances showed the same change in slope (9). In many instances ionized field charging occurred to such a degree that spray current polarity reversals and zero spray currents actually occurred at high voltages as for model A in Figure 7.

Reverse ionization from the grounded nozzle side of the inducing field was not thought to have occurred since such a discharge would have supplemented induction charging instead of opposing it.

The origin of corona at the induction electrodes was determined to be water discharge points which formed when the electrodes became wet. When a wet spherical induction electrode was observed at high potentials in darkness with the spray on, the blueish corona light could be seen on a part of the sphere facing the nozzle. As the head potential increased, the area covered by the corona increased. Just prior to spark breakdown, the corona enveloped nearly all of the hemispherical area facing the nozzle. When enough moisture collected on the sphere to form a drop at the bottom, the drop would become sharply peaked, and corona could be seen coming from it as well as an ejection of highly charged droplets torn from its disrupted surface.

Time exposure photographs of corona from a wet 5/16 inch diameter spherical electrode were made both for the metal and the dielectric nozzles. One photograph was made for each nozzle in which the film was exposed by only the light from the corona itself in the absence of any other illumination; these are Figures 8-a and 8-c. Further, one photograph was made for

(a) Dielectric nozzle,
     30 second exposure,
     no flash
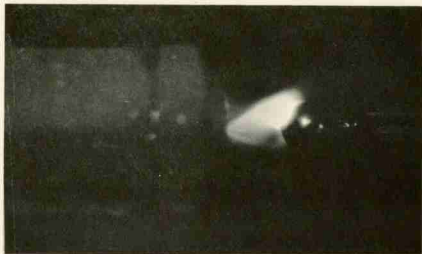
(b) Dielectric nozzle,
     30 second exposure,
     electronic flash
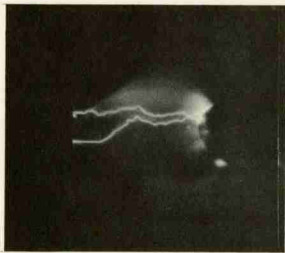
(c) Metal nozzle,
     30 second exposure,
     no flash
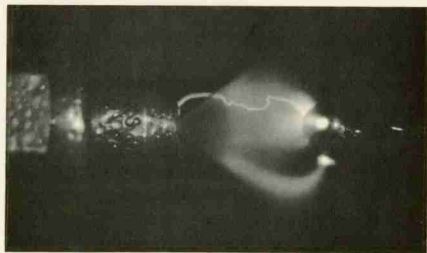
(d) Metal nozzle,
     45 second exposure,
     electronic flash

Figure 8 Time exposures of corona from a wet 5/16 inch diameter
          spherical induction electrode for both metal and dielectric
          nozzles while spraying

each nozzle in the same manner as before, except that an electronic flash
was used at the end of the exposure to illuminate the nozzle and electrode;
these are Figures 8-b and 8-d. All these photographs were made just below
spark-breakdown voltages. Near the end of the exposures for the metal
nozzle, the voltage was slowly increased to include the spark-breakdown
paths in Figures 8-c and 8-d. Also the corona which occurred from the
liquid drop that formed at the underside of the sphere is well shown by
these last two figures.

Charging Efficiency

It was desirable to know the value of the maximum charge experimentally
induced onto spray droplets of this study and to compare such a value with
that given by an equation derived for the theoretical maximum droplet
charge (see appendix). The model B combination spherical-toroidal induction
head was chosen to be evaluated since its spray discharge current of -3.60
microamperes at +4 kv was the greatest produced by induction (See Figure 7).
The number of 51 micron diameter droplets leaving the nozzle was calculated
to be about 62.2×10^6 drops/sec. Since no knowledge of the droplet size
distribution was at hand, this calculation required the assumption that the
median number diameter equalled the mass average diameter; that is, the
assumption of a spray of uniform droplet diameter of 51 microns was made.
Under this assumption the charge carried per droplet was calculated to be
5.8×10^{-14} coulombs or 3.61×10^5 electronic charges. The theoretical
maximum droplet charge for a 51 micron droplet was calculated to be 2.28
$\times 10^{-12}$ coulombs or 1.42×10^7 electronic charges. Thus, the experi-
mentally attained droplet charge was estimated to be about 3% of the
theoretical maximum.

The spray was not of a uniform size, and it was realized that the above assumption subjected the results to error which increased as the dispersion of drop diameters about a mean or median diameter increased. However, the experimental droplet charge calculated using such an assumption established a lower limit on the charge actually attained.

Field Test

Three of the model A induction heads were fitted to the spray boom of a high clearance field sprayer as shown in Figure 6. A portable, 14 kv, direct current power supply mounted on the spray rig was operated from the engine battery to provide the head potential. A voltage divider circuit was incorporated on the input side of the power supply so that the input voltage could be adjusted to provide a $+7$ kv output voltage. Optimum inductive spray charging for this model A electrode had been previously found to occur at this output voltage as shown by Figure 7.

Three plots composed of three rows each of mature cotton plants were each treated with both charged and uncharged sprays of a well agitated aqueous suspension of fluorescent zinc orthosilicate (Sylvania 2282). Fifteen plants were then randomly sampled from each plot, and a leaf was randomly removed from the bottom, middle, and top sections of each plant. A group of leaves which ranged from practically no fluorescence to total surface fluorescence was chosen for a set of standards, and the sampled leaves were visually compared and ranked with the standards under ultra-violet light (2537 Angstrom units) in a dark chamber. Four observers, all unaware of the treatment being evaluated, ranked the samples. The top and bottom surfaces of the leaves were evaluated separately. Each standard leaf was assigned a numerical value according to its amount of fluorescence; and results of ranking were, thus, weighted. The total sum of squares was

partitioned into sums of squares for location on plant, replication, and treatment. Spray charging could not be declared to significantly increase leaf top coverage even at the 10% level of F. However, inductive spray charging did significantly increase the coverage of the bottom side of leaves at the 10% level of F. An average increase of 3.8 times occurred in the leaf bottom coverage due to charging the spray.

The field test left something to be desired; electrode potential could not be held constant at the optimum value of +7 kv during the test due to a conductive path being formed to ground potential when the plexiglas head insulators became damp. The voltage fluctuated between +4 and +7 kv.

Summary and Conclusions

In order to improve the coverage of plant surfaces by pesticide sprays, through the action of electrostatic precipitation, the problems encountered in the charging of sprays by electrostatic induction were investigated.

The charge induced onto spray from a dielectric nozzle by a 5/16 inch induction sphere set at 9 mm gap was found to be significantly greater than for a metal nozzle at the 1% probability level of Student's t for voltages of 1.5 to 7.0 kv inclusive. No significant difference in charging for the two kinds of nozzles was found even at the 10% level of t for voltages of 0.25 to 1.00 kv inclusive and for 8.0 kv. Thus, it was concluded that dielectric nozzles were superior for inductive spray charging.

Two models of a combination spherical-toroidal induction head of the same basic design were tested using a hollow cone spray nozzle. The maximum spray discharge currents attained inductively were -3.60 microamperes at +4 kv for the model of smaller dimensions and -2.70 microamperes at +7 kv for the model of larger dimensions.

Ionized field spray charging by corona from water discharge points on the induction electrodes was found to oppose induction spray charging. In some instances, these two counteracting charging phenomena exactly nullified each other as, for example, at +12.2 kv for the combination induction head model A; and a polarity reversal of the spray current occurred. It was concluded that in order to significantly increase the net charge induced onto sprays, the problem of the opposing ionized field charging from liquid on the induction electrodes would have to be overcome.

The value of the maximum charge experimentally induced onto spray droplets of this study was calculated to be 5.8×10^{-14} coulombs or 3.61×10^{5} electronic charges/droplet. Since this calculation required the assumption of the median number droplet diameter of 51 microns being equal to the mass average diameter, and since the spray was known not to be of constant diameter, this calculated droplet charge established the lower limit of the charge actually attained. The theoretical maximum charge for 51 micron diameter droplet as calculated from the derived equation for theoretical maximum droplet charge equalled 2.28×10^{-12} coulombs or 1.42×10^{7} electronic charges. Thus, it was concluded that the maximum experimentally attained droplet charge was at least about 3% of the theoretical maximum, and probably more.

Inductive spray charging significantly increased the spray coverage of the bottom side of cotton leaves at the 10% probability level of F. An average increase of 3.8 times occurred in the leaf bottom coverage due to charging the spray.

LIST OF REFERENCES

1. Allen, K. R. and K. Phillips. 1959. Effect of humidity on the spark-breakdown voltage. Nature. 183:174-175.

2. Blanchard, D. C. 1955. Electrified droplets from the bursting of bubbles at an air-sea water interface. Nature. 175:334-336.

3. Brooks, F. A. 1947. The drifting of poisonous dusts applied by airplanes and land rigs. Agricultural Engineering. 28:233-239.

4. Chapman, S. 1934. The charges on droplets produced by the spraying of liquids as revealed by the Millikan oil drop method. Physics (J. Appl. Phys.). 5:150.

5. Cobine, J. D. 1958. Gaseous Conductors. Dover Publications, Inc., New York.

6. English, W. N. 1948. Corona from a water drop. Physical Review. 74:179-189.

7. Ennis, W. B., Jr. and R. E. Williamson. 1963. Influence of droplet size on effectiveness of low-volume herbicidal sprays. Weeds. 11:67-72.

8. Franck, S. 1931. Messentladungstrecken. Springer-Verlag, Berlin.

9. Law, S. E. 1964. The charging of liquid spray by electrostatic induction. Unpublished M.S. thesis, Department of Agricultural Engineering, North Carolina State University, Raleigh.

10. Lewis, A. B. 1939. The effects of irradiation, humidity, and sphere material on the spark-over voltage of the two-centimeter sphere gap. J. Appl. Phys. 10:573-577.

11. Peek, F. W. 1929. Dielectric Phenomena in High-Voltage Engineering. McGraw-Hill Book Company, Inc., New York.

12. Ryan, H. J. 1904. The conductivity of the atmosphere at high voltages. Trans. Am. Inst. Elec. Engr. 23:101-134.

13. Splinter, W. E. 1955. Deposition of aerial suspensions of pesticides. Unpublished PhD thesis, Department of Agricultural Engineering, Michigan State College, East Lansing.

14. Telford, J. W., Thorndike, N. S., and E. G. Bowen. 1955. Coalescence between small water drops. Roy. Meteor. Soc. Quart. J. 81:241-250.

15. Vonnegut, Benard and R. L. Neubauer. 1952. Production of monodisperse liquid particles by electrical atomization. J. Colloid Sci. 7:616-622.

16. Wampler, E. L. and W. M. Hoskins. 1939. Factors concerned in deposit of sprays; the role of electrical charges produced during spraying. J. Econ. Entom. 32:61-69.

17. Zeleny, J. 1914. On the conditions of instability of electrified drops with applications to the electrical discharge from liquid points. Proc. Cambridge Philos. Soc. 18:71-83.

APPENDIX

Theoretical Maximum Droplet Charge

The electric field intensity immediately off the surface of a spherical conducting droplet is obtainable through the use of Gauss' law. That is

$$\int_S \vec{E} \cdot \vec{n} \, dS = \frac{4\pi Q}{\epsilon} \tag{1}$$

where $\vec{E}$ = electric field intensity (statvolts/cm)

$\vec{n}$ = unit vector normal to surface

Q = droplet charge (statcoulombs)

ϵ = absolute permitivity of air = $1 \frac{statcoulomb^2}{dyne \ cm^2}$

The integration of equation (1) is performed over the closed spherical surface of radius r. Just off of a conducting sphere of uniform surface charge density, the intensity vector $\vec{E}$ is everywhere equal in magnitude and normal to the surface. Hence, for a droplet of radius r, equation (1) reduces to

$$E_r 4\pi r^2 = \frac{4\pi Q}{\epsilon}$$

$$E_r = \frac{Q}{\epsilon r^2} \tag{2}$$

where E_r = magnitude of field intensity immediately off droplet surface (statvolts/cm).

The dielectric strength of the air surrounding the droplet determines the upper limit for E_r; and, hence, it determines the theoretical maximum charge for a droplet of radius r by equation (2). It is known that the

dielectric strength of air is considerably greater than 30 kv/cm at the
surface of small conductors (5, 11, 12). In order for electrons and ions
to be accelerated to ionizing energies, they must be acted upon over a
finite distance by a field of at least 30 kv/cm. With the very rapidly
outward diverging fields of small conductors, this requires that the field
intensity immediately of the surface greatly exceed 30 kv/cm. The empirical
equation (11)

$$E_c = 27.2 \ (1 + \frac{0.54}{\sqrt{r}}) \tag{3}$$

where E_c = surface gradient at breakdown (kv/cm)

r = conductor radius (cm)

gives the necessary surface gradient for breakdown around sperical conductors.
The equation is known to hold true down to $r = 0.159$ cm, and it will be
assumed to apply to radii occurring in the droplet spray spectrum.

When the surface breakdown gradient given by equation (3) is converted
to statvolts/cm and substituted for E_r in equation (2), the following equation
for theoretical maximum droplet charge $Q_{max.}$ is obtained

$$Q_{max.} = 90.7 \ (1 + \frac{0.54}{\sqrt{r}}) \ r^2 \tag{4}$$

where $Q_{max.}$ = maximum droplet charge (statcoulombs)

r = droplet radius (cm).

Our research activity in methane gas generation is just in the initial stages and our objectives very narrow. However, I am enclosing an abstract of a paper that we will be giving at an upcoming professional meeting. This will give you some indication of our activity and the type of information we are trying to determine.

Additionally I am enclosing a reference listing for material on methane gas generation that may be helpful. You will find instructions for working models in the publication from the New Alchemy Institute and will also find the Mother Earth Society in Hendersonville, N. C., to be very helpful.

We anticipate expanding this methane generation research and will keep you informed as research results are published.

Sincerely,
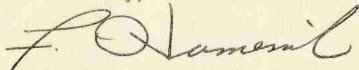
Frank J. Humenik, In Charge, Extension
Biological & Agricultural Engineering

FJH:s
Enc.

METHANE PRODUCTION FROM SWINE WASTE WITH A SOLAR REACTOR

R. Parker, F. Humenik, R. G. Holmes, M. R. Overcash, and L. Safrit, Jr.
Biological and Agricultural Engineering
North Carolina State University
Raleigh, North Carolina

A methane generator has been developed to incorporate the sun's energy and biological degradation of swine waste into a useful product while at the same time eliminating or mitigating several nuisances and limitations associated with conventional lagoons. This reactor has advantages over lagoons in that there is no loss of ammonia nitrogen from the system because it is trapped in removed condensate, seasonal weather influences are minimized, odors are controlled, and energy recovery capabilities exist. Anaerobic degradation of sewage sludge to methane and carbon dioxide in municipal treatment plant digesters and even individual septic tanks is a well established and understood biological process. Gas from individual digesters has been utilized extensively in India. Basic principles concerning methane digesters for fuel gas and fertilizer with complete instructions for two working models was presented by Fry (1963). Cross and Duran (1970) presented data for laboratory studies on the anaerobic decomposition of swine waste.

Initial Prototype

Concepts for solar stills presented by Jackson and Van Bavel (1966) and Hay (1966) directed construction of the first two hundred (200) gallon field prototype detailed in Figure 1. The "funnel shaped" 6 mil polyethylene top for this cylindered reactor had a drain for rainwater removal at the bottom center. A funnel for condensate collection and removal was plumbed in association with the rainwater drain.

Test Results

The condensate was clear and had an ammonia concentration of about 400 mg/1, chemical oxygen demand (COD) of 30 mg/1, and total organic carbon (TOC) of 0 mg/1, but only a fraction of the expected amount was collected. The polyethylene top material deteriorated rapidly, becoming dark brown and almost opaque within one month, apparently due to ultra-violet radiation and the corrosive environment within the reactor. Thus the polyethylene was removed and a similar 10 mil vinyl "funnel shaped" top was installed. The vinyl material also became discolored and almost opaque within a month.

Gas production of about of about 90 liters per week was considerably below expected rates (Loehr, 1968). The relative concentration of methane increased until analyses made with the Orsat gas apparatus indicated 35% methane and 20% carbon dioxide prior to rupture of the vinyl top. This unit had been charged initially with 200 gallons of swine manure pit slurry diluted to a COD of 3800 mg/1. Reactor fluid was maintained at about 95° F with a hot water heater system. Reactor liquid hydrogen ion concentration initially was pH = 7.4 and varied from 6.4 to 7.8 during the six weeks of operation. It was apparent that this process had sufficient promise to justify construction of a similar reactor that would provide a better research tool.

Field Model

The currently studied 500 gallon reactor (Figure 2) was developed with new and more flexible operating capabilities. The square tank reactor was fabricated with an inverted pyramid bottom for sludge removal and a top sloped at 20° for better sun

penetration and condensate removal. The top was constructed to allow investigation of two 2' x 4' transparent top materials simultaneously, the first two being glass and plexiglass. The reactor fluid is mixed with a 5 HP manure handling pump for 3 inch solids that operates by a timer control 2 minutes each 15 minutes. The reactor diagram presented in Figure 1 shows plumbing details. No supplemental heating was provided, but 6 inches of styrofoam insulation was placed around the total side wall area.

Results

The present insulation scheme has not been adequate to maintain an optimum temperature of 98° F during cold periods, and the reactor fluid temperature dropped to 65° F. At present the styrofoam is completely covered with a layer of black polyethylene to reduce air passage between styrofoam sheets.

Gas is removed from the system when internal pressure exceeds the resistance of the wet test meter used for volume measurements. Gas production from the unit has been as high as 650 liters per week with a gas composition of approximately 50% CH_4 and 20% CO_2; however steady state operation has not yet been achieved due to both operational difficulties and unavoidable variations in waste strength. At present arrangements have been made to dilute the manure pit slurry to a COD of about 40,000 mg/l to allow a relatively constant weekly load of 50 gallons.

The top material of glass and plexiglass has not become visibly deteriorated during the current 6-month operational period. A photometer inserted through an access port shows no difference or reduction in amount of sunlight transmitted for both materials in spite of the abundance of water droplets on the underside of the plexiglass. Condensate removal of about 2 gallons per week from the glass is generally about twice the quantity from the plexiglass but much lower than the value of 1 gallon per 8 square feet per day from glass covered greenhouse stills. Visual observations indicate that a large amount of the condensate on the plexiglass never reaches the collection tray due to the formation of large drops which fall back into solution.

CONCLUSIONS

The feasibility of a solar still reactor for anaerobic methane production without supplemental heating has been sufficiently demonstrated with a model field unit to justify continued investigation of design and operational criteria pursuant to rigorous evaluation of the technical and economic suitability of this utilization-treatment concept.
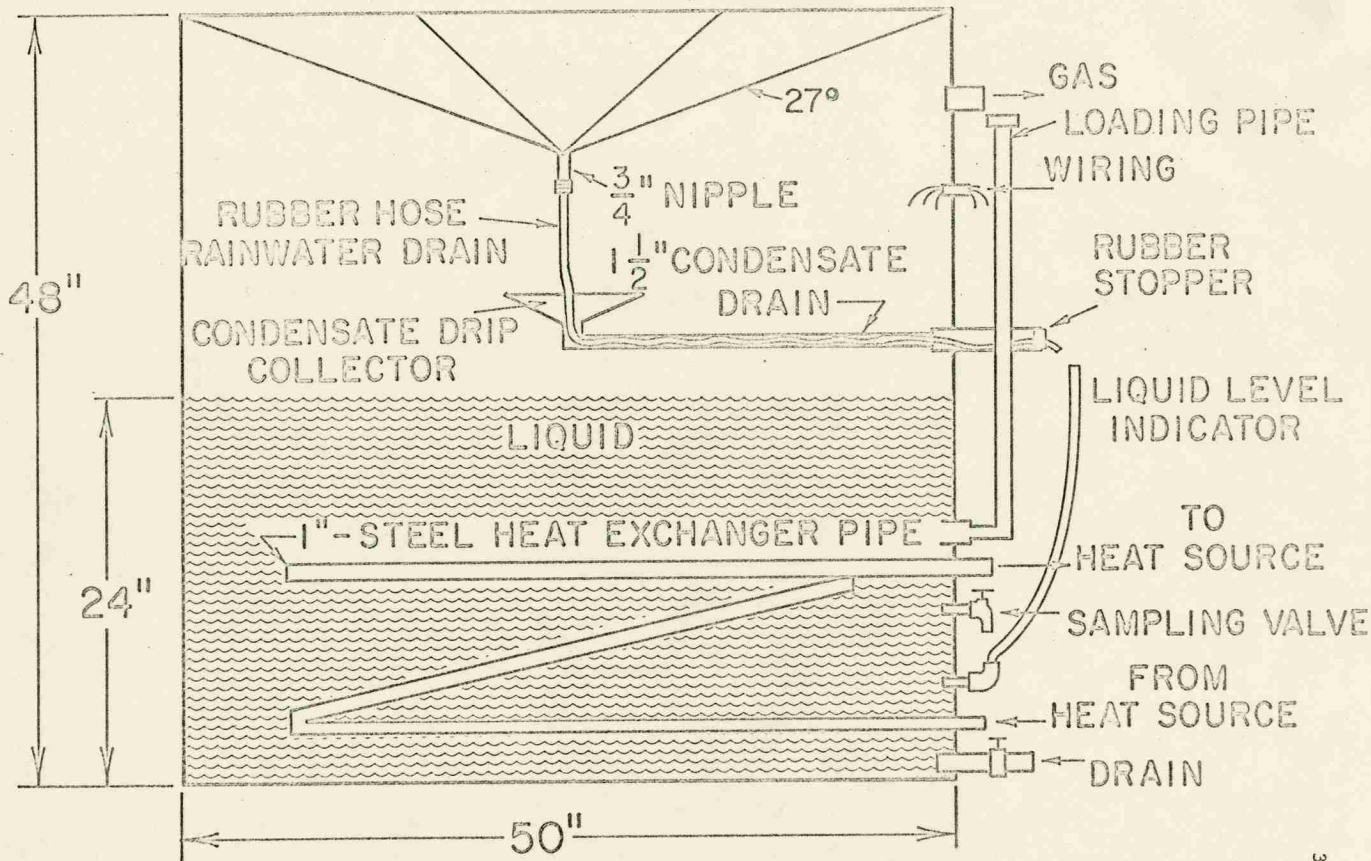
Figure 1. Details of 200 gallon prototype solar methane generator.

ACCESS PORT W/ VINAL TUBES

2'-0"   2'-0"

PLEXIGLAS TOP

GLASS TOP

1'-5"

20°

LIQUID LEVEL

CONDESATE COLLECTOR

4'-0"

SAMPLING PORT

2" PIPE FOR MIXING - FROM PUMP

CONDESATE REMOVAL PORTS ½" PIPE

2½" x 2½" x ¼" SUPPORT ANGLES

SAMPLING PORT

2'-6"

1'-8"

GAS REMOVAL PIPE

3" TO PUMP

4'-0"

TO WET TEST METER

4'-0"
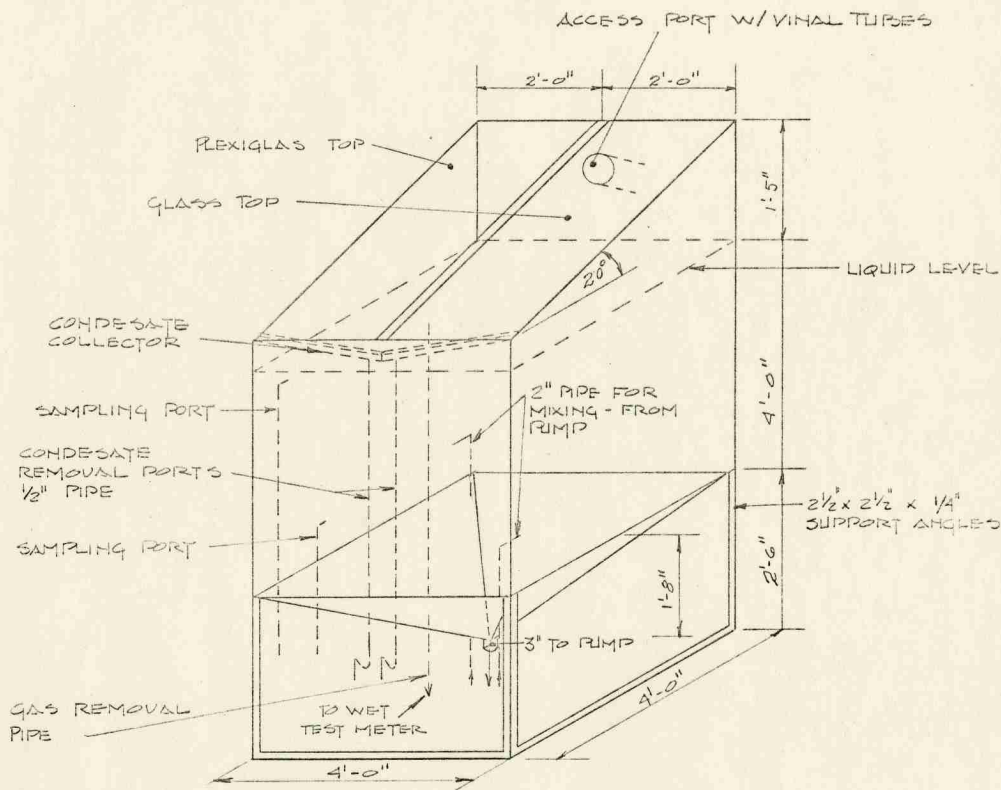
NOTE: ALL PIPE SHOWN AS SINGLE DOTTED LINE

Figure 2.   Schematic of 500 gallon solar methane generator

REFERENCES

1. Cross, O. E. and Alvato Duran. 1970. Anaerobic decomposition of swine excrement. Transactions of the ASAE 13(3):320-325.

2. Fry, John L. Methane digesters for fuel gas and fertilizer with complete instructions for two working models. New Alchemy Institute Newsletter No. 3. Spring 1973. Box 432, Woods Hole, Massachusetts 02543.

3. Hay, Harold R. V-cover solar stills. Sun at Work, 2nd Quarter, 1966.

4. Jackson, Ray D. and C. H. M. van Bavel. Solar distillation of water from soil and plant materials: A simple desert survival technique. Science 149(3690): 1377-1379. September 17, 1966.

5. Loehr, R. C. 1968. Anaerobic lagoons: Considerations in design and application. Transactions of the ASAE 11(3):320-322.

Methane Production From Swine Waste With a Solar Reactor

R. Parker, F. J. Humenik, R. G. Holmes and M. R. Overcash
Biological and Agricultural Engineering Department
N. C. State University - Raleigh

A solar still type reactor for the anaerobic fermentation of swine waste incorporating methane recovery and condensate removal has been developed. The design and operation of a 500 gallon field unit has been directed by preliminary prototype work.

Solar radiation is utilized to maintain liquid temperatures suitable for mesophilic fermentation. The suitability of various rigid and flexible cover materials for condensate collection and energy transmittance have been evaluated. A 5 h.p. centrifugal solids handling pump has been employed to study different mixing strageties.

Material balances for COD, TOC and nitrogen are continuously recorded pursuant to definition of steady-state operation. The composition and quantity of gas produced are recorded. Additionally, the quality and quantity of condensate removed are measured and included in mass balance considerations. Economic evaluations are being made to access process cost.

Mass balance data will be evaluated to determine reaction kinetics for investigated operational conditions. Optimization procedures will consider relationship between maximum methane production, stabilization of waste input and residue volume reduction.

Design considerations and operational characteristics for the prototype and field unit will be discussed. Preliminary analytical data for the 500 gallon solar still methane generator will be presented and evaluated.

PARTIAL REFERENCE LISTING FOR METHANE GAS GENERATION

AND PERTINENT MATERIAL ON SOLAR STILLS

Jackson, Ray D., and C. H. M. van Bavel. Solar distillation of water from soil and plant materials: A simple desert survival technique. Science 149(3690):1377-1379. September 17, 1966.

Hay, Harold R. V-cover solar stills. Sun at Work, 2nd Quarter, 1966.

Singh, Ram Bux. Building a bio-gas plant. Compost Science, Marth-April, 1972.

Zeikus and R. S. Wolfe. Methanobacterium thermautotrophicus sp. n., an anaerobic, autotrphoic, extreme thermophile. Journal of Bacteriology 109(2):707-713. February 1972.

Cross, O. E. and Alvato Duran. Anaerobic decomposition of swine excrement. Transactions of the ASAE, Pages 320-325. 1970.

Singh, Ram Bux. Bio-gas plant - generating methane from organic wastes. Gobar Gas Research Station. Ajitmal, Etawah (U.P.) India

Methane digesters for fuel gas and fertilizer with complete instructions for two working models. New Alchemy Institute Newsletter No. 3. Spring 1973. Box 432, Woods Hole, Massachusetts 02543.

Mother Earth, P.O. Box 70, Hendersonville, N. C. 28739
(This group has extensive technical and popular material on both methane generation and trapping solar energy.)

1. TITLE: Objective measurement of certain quality factors in peanuts.

2. OBJECTIVES:

    a. Correlate various physical measurements with observable quality
        characteristics and known curing treatments.

    b. Determine the structural and compositional changes in peanut
        kernels responsible for any differences in physical measurements.

    c. Develop a rapid means of making objective measurements indicated
        by the study.

3. REASONS FOR UNDERTAKING THE STUDY:

    The change from the stackpole method of harvesting to more mechanized
    methods seems to be dependent upon a method for curing peanuts in bulk.
    This method of curing demands good management. If poor management is
    used and the peanuts are subjected to high temperature, undesirable
    changes in their flavor and other characteristics will be developed.

    At present, the authors are unaware of any objective measurements
    which can be correlated to "off flavor". In addition to change in the
    flavor there are possibly other undesirable changes in the peanut ker-
    nel which are produced by high temperature curing and which could be
    detected and described by means of physical measurements. Any advance
    in the measurement of changes in peanuts produced by various curing
    methods would be of great value both to the research program in pea-
    nut curing as well as through the development of confidence on the part
    of the entire industry which must maintain a high level of quality in
    its products at every level of production.

4. PREVIOUS WORK:

    The Biological Sciences Branch of the Agricultural Marketing Service
    has conducted studies on the correlation of light transmittance to
    "off flavor" in peanuts. Their results show a correlation between
    "off flavor" and light transmittance, but there is also an effect of
    maturity on light transmittance which makes the reading undependable
    as an index of "off flavor" until further modifications are made.

    The Southern Regional Laboratory of USDA has employed a method of
    paper chromatography to identify certain flavor constitutents of pea-
    nuts but those constitutents are not believed to be those responsible
    for the "off flavor" produced by high temperature curing.

    Certain components have been removed from peanuts by vacuum distilla-
    tion at North Carolina State College. The distillate has been analysed
    by chemical and light transmittance methods. Both methods agreed that

aldehydes were present but other components responsible for "off flavor" were not identified. Other chemical studies carried on over a period of years have been unsuccessful in identifying the cause of "off flavor" in peanuts.

Microscopic studies made at North Carolina State College reveal no differences between peanuts cured at high or low temperatures.

5. PROCEDURE:

Initially, peanuts with varying degrees of "off flavor" and having had various curing treatments will be subjected to such physical measurements as light transmittance of the kernel and its distillate, the dielectric properties of the kernel, response of the peanut to ionizing rays and the fluorescence of the kernel. Gas chromotography will also be employed to detect and identify components of the distillate from the kernels.

Subsequently, any of the above or other measurements which show promise as being indicative of quality will be more thoroughly developed and evaluated. Any findings will be subjected to thorough chemical and physical analysis in an attempt to verify any structural or compositional changes indicated.

Finally, any measurement showing a definite correlation with quality factors will be adapted, if possible, to be a rapid means of making quality determinations.

6. Item No. 7 - Support and Responsibility. *) all caps*

<u>Best Foods, Division of Corn Products Company</u>

The Best Foods, <u>Division of Corn Products Company</u>, agrees to place at
the disposal of the N. C. Agricultural Experiment Station the sum of $3,000
for the year beginning   and ending   .
This contribution will be used in part for the employment of a graduate student
or other personnel to assist with the project and for other expenses incident to
carrying out part of the responsibilities set forth in this agreement.

Financial support furnished by Best Foods in subsequent years will be xxxxx
reviewed annually and agreed upon at the time of renewal of agreement. Any
funds furnished to support the project and not used in any one year will remain
in the account and be available for use on the project in subsequent years.

<u>Department of Agricultural Engineering</u>

The N. C. Agricultural Experiment Station agrees to supply the necessary
leadership, personnel and physical facilities for carrying out this project.

Item No. 8 - Reports *) all caps*

The N. C. Agricultural Experiment Station will furnish to the cooperator a
written report on the investigations covered by this agreement each year or sooner
if requested.   Rights to publication or formal release of the results will be
retained by the N. C. Agric. Exp. Station and no publication or formal release
of the data will be made without its knowledge and consent.   In all publications
the cooperation of the Best Foods will be acknowledge.   Provisions may be made for
withholding publications for a limited time in the interest of Bests Foods Co.

Item No. 9 - ~~Name of~~

The Name of the N. C. Agric. Exp. Station or any of its staff are not to be used in any commercial advertisements relating to this ;work unless written permission is secured.

Item No. 10.

Neither party to this agreement assumes any responsibility for bodily ~~exxxxgxies~~ injuries to the employees of the other party or its cooperators while working on the project, nor for damage to the project of other parties working on the project.

Item ~~No.~~ 11 - Duration:] all caps

This memorandum of understanding shall continue in effect to _____ and from year to year thereafter unless cancelled by either party upon three months notice. It is the intent, however, of both parties that this agreement run for two years--a time necessary for the graduate student to complete the degree and to make a meaningful ~~satisfactory~~ contribution ~~to the project.~~